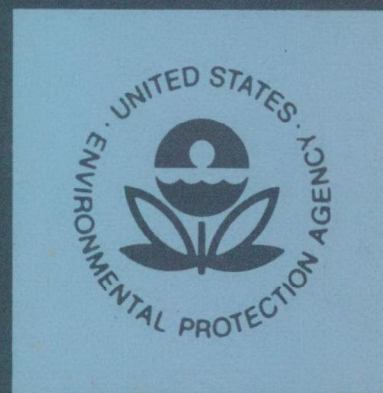


Environmental Protection Technology Series

VERSATILE  
GAS FILTER  
CORRELATION SPECTROMETER



U.S. Environmental Protection Agency  
Office of Research and Development  
Washington, D. C. 20460

VERSATILE GAS FILTER  
CORRELATION SPECTROMETER

by

*Francis*  
D. E. Burch, F. J. Gates, D. A. Gryvnak  
and J. D. Pembrook *John*  
Aeronutronic Ford Corporation  
Aeronutronic Division  
Newport Beach, California 92663

Contract No. 68-02-1227

Project Officer

F. M. Black  
Emissions Measurement and Characterization Division  
Environmental Sciences Research Laboratory  
Research Triangle Park, North Carolina 27711

U.S. ENVIRONMENTAL PROTECTION AGENCY  
OFFICE OF RESEARCH AND DEVELOPMENT  
ENVIRONMENTAL SCIENCES RESEARCH LABORATORY  
RESEARCH TRIANGLE PARK, NORTH CAROLINA 27711

U.S. Environmental Protection Agency  
Sam Nunn Atlanta Federal Center  
Region 4 Library  
61 Forsyth Street S.W.  
Atlanta, Georgia 30303

## DISCLAIMER

This report has been reviewed by the Environmental Sciences Research Laboratory, U.S. Environmental Protection Agency, and approved for publication. Approval does not signify that the contents necessarily reflect the view and policies of the U.S. Environmental Protection Agency, nor does mention of trade names or commercial products constitute endorsement or recommendation for use.

## RESEARCH REPORTING SERIES

Research reports of the Office of Research and Development, U.S. Environmental Protection Agency, have been grouped into five series. These five broad categories were established to facilitate further development and application of environmental technology. Elimination of traditional groupings was consciously planned to foster technology transfer and a maximum interface in related fields. The five series are:

1. Environmental Health Effects Research
2. Environmental Protection Technology
3. Ecological Research
4. Environmental Monitoring
5. Socioeconomic Environmental Studies

This report has been assigned to the ENVIRONMENTAL PROTECTION TECHNOLOGY series. This series describes research performed to develop and demonstrate instrumentation, equipment and methodology to repair or prevent environmental degradation from point and non-point sources of pollution. This work provides the new or improved technology required for the control and treatment of pollution sources to meet environmental quality standards.

This document is available to the public through the National Technical Information Service, Springfield, Virginia 22161.

## CONTENTS

	<u>Page</u>
List of Figures	iv
List of Abbreviations and Symbols	v
Acknowledgements	vii
I Introduction	1
II Summary	3
III Conclusions	5
IV Recommendations	7
V Layout and Spectroscopic Principles	9
VI Formaldehyde Gas-Filter Cell	21
VII Multiple-Pass Sample Cell	27
VIII Grating Section	33
IX Electronics and Processing of Detector Signal	41
X H <sub>2</sub> O Monitor	45
XI Results of Formaldehyde Tests	49
XII Measurements of NH <sub>3</sub> and Vinyl Chloride Near 1000 cm <sup>-1</sup>	59
XIII References	67

## LIST OF FIGURES

<u>Number</u>		<u>Page</u>
1	Optical Diagram and Layout of the Instrument	10
2	Photograph of the Instrument	11
3	Two drawings of the Formaldehyde Gas-Filter Cell	22
4	Plot of the Pressure of Formaldehyde Vapor vs the GFC Temperature	25
5	Photographic View of One End of the Multiple-Pass Sample Cell from the Back Side of the Instrument	28
6	Sample Inlet and Optical Diagram of the Bypass Optics Assembly	29
7	Multiple-Pass Optical System in the Sample Cell	31
8	Optical Diagram of the Retroreflector-Grid Assembly	34
9	Optical Diagram Defining Angles that Relate the Grating Position to the Wavelength of Energy Passed by the Grating Assembly	35
10	Calibration Curves Relating the Grating Drive Counts to Wavelength and to Wavenumber	37
11	Curves of $\delta\nu/\delta g$ and $\cos \alpha/\cos \beta$ vs Wavenumber for the Three Gratings	39
12	Plot of Trapezoidal Slit Function	40
13	Block Diagram of Electronics	42
14	Two Optical Diagrams of the H <sub>2</sub> O Monitor	46
15	Diagram of the Receiving Optics for the H <sub>2</sub> O Monitor	47
16	Spectral Curves of Transmittance for Formaldehyde and Five Hydrocarbons	50
17	Recorder Plots of the Noise on the Signal Output for Various Operating Conditions	57
18	Spectral Curves of Transmittance of NH <sub>3</sub> , Vinyl Chloride, and Ethylene Between 920 and 985 cm <sup>-1</sup>	60

## LIST OF ABBREVIATIONS AND SYMBOLS

### ABBREVIATIONS

GFC	--gas-filter cell, also called correlation cell
T	--transmittance at a particular wavenumber (or wavelength) that would be measured with a spectrometer having infinite resolving power. Subscripts indicate the transmittance of different components or gas samples. $\bar{T}$ indicates the average transmittance over a specified interval.
$T_s$	--transmittance of the sample gas being analyzed
$T_f$	--transmittance of the spectral bandpass filter
$T_g$	--transmittance of the gas in the GFC
$T_{at}$	--transmittance of an attenuator, assumed to be constant over the spectral bandpass of interest
$\bar{T}_{g,s}$	--average transmittance of a sample as measured with the beam of energy passing through the GFC. (Equation 6)
$\bar{T}_{at,s}$	--average transmittance of a sample as measured with the beam of energy passing through the attenuator. (Equation 7)
A	--absorptance, $A = 1 - T$ . Subscripts used with A are the same as those used with T
$\nu$	--wavenumber of radiant energy ( $\text{cm}^{-1}$ )
$\lambda$	--wavelength of radiant energy expressed in micrometers ( $\mu\text{m}$ )
$\nu_c, \lambda_c$	--wavenumber, or wavelength, of the center of a specified interval
$f_c$	--carrier frequency (high) (Hz)
$f_a$	--alternator frequency (low) (Hz)
p	--partial pressure of a particular gas species (atm)
P	--total pressure of a gas mixture (atm)
$l$	--geometrical path length of the radiant energy beam through a gas sample (cm)
c	-- $p/P$ , concentration of a gas species, usually expressed in parts per million (ppm) or percent
u	-- $p\ell$ (atm cm), absorber thickness of a particular gas species. One atm cm is equivalent to $10^4$ ppm meters
$\bar{k}_s$	--average absorption coefficient of a sample over a specified interval $(\text{atm cm})^{-1}$ , (Equation (21))

M --constant that accounts for aperture size and field-of-view in radiant energy beam, (Equation (1))

R --responsivity of the detector at the wavenumber of interest

$N_{\nu}$  --spectral emissivity of the radiant energy source at the wavenumber of interest

$E_g$  --the amount of radiant energy chopped at 360 Hz that is incident on the detector during the GFC-half of the alternator cycle, (Equation (1))

$E_{at}$  --the amount of radiant energy chopped at 360 Hz that is incident on the detector during the attenuator-half of the alternator cycle, (Equation (2))

$\Delta$  -- $E_g - E_{at}$  (Equation (10))

$\Sigma$  -- $E_g + E_{at}$  (Equation (11))

$V_c$  --voltage component of amplified detector signal at carrier frequency  $f_c$

$V_a$  --voltage component of amplified detector signal at alternating frequency  $f_a$

$V'$  -- $V_a/V_c$ , normalized voltage. Normalization is made so that  $V' = 1$  when there is 100% modulation of the beam at frequency  $f_a$ . See Equation (12) and related text

AGC --automatic gain control.

$C_e$  --correlation efficiency (Equations (13) and (15))

F -- $\lim_{u \rightarrow 0} \frac{V'}{u}$  Pembroke Factor  $(\text{atm cm})^{-1}$ , (Equation (19))

D.R. --discrimination ratio, ratio of the concentration of an interfering gas species to the concentration of the species being measured that produces the same reading. This ratio may be positive or negative.

f --focal length of a mirror or lens (cm)

$\alpha, \beta, \theta, \phi$  --angles relating position of grating to the incident and diffracted beams (see Equations (23) through (26))

D --distance between adjacent grooves of a grating

$W_n, W_g$  --physical width of the entrance slit and opening in the grid, respectively

g --distance measured at the grid in the direction of the dispersion (mm)

## ACKNOWLEDGEMENT

The authors would like to express their appreciation for the cooperation and assistance of four co-workers. Mr. Wayne Leicht and Mr. Kim Choy designed many of the components and assisted in acquiring the purchased parts. Mr. Oliver Pacific and Mr. George Hart performed most of the machine shop work and were very helpful in assembling and checking out the instrument.

THIS PAGE LEFT BLANK INTENTIONALLY

## SECTION I

### INTRODUCTION

During some experimentation a few years ago with gas-filter correlation instruments we found that instrument stability, sensitivity and discrimination could be improved significantly by carefully selecting the spectral bandpass. Under two previous contracts with the Environmental Protection Agency,<sup>1,2</sup> Aeronutronic designed and built two gas-filter correlation instruments, each of which included a small grating assembly that made it possible to select the optimum bandpass. Commercially available interference filters frequently cannot be obtained with the optimum transmission characteristics. The grating assemblies are based on a principle developed by us<sup>3</sup> for an instrument that employed a prism as a dispersing element instead of a grating. The width and the center position of the spectral bandpass can each be adjusted independently while measuring the sensitivity and interference as the instrument is being assembled and tested. Thus, the optimum bandpass can be determined with very good precision.

A single grating assembly can be used to provide the desired spectral bandpasses for two or more different gas species. The grating assembly in the instrument described in Reference 1 transmits a spectral band near 3.3  $\mu\text{m}$  for the measurement of  $\text{CH}_4$  and another band near 4.6  $\mu\text{m}$  for the measurement of  $\text{CO}$ . A single grating assembly in the instrument described in Reference 2 transmits a spectral band for  $\text{CO}$  and one for  $\text{NO}$ . Each band consists of several very narrow intervals, each of which includes a strong absorption line of the gas species being measured. All of the optical components in these grating assemblies were bonded permanently in place so that the bandpasses could not be shifted after the alignment had been completed.

- 
1. Burch, D. E., and J. D. Pembrook. "Instrument to Monitor  $\text{CH}_4$ ,  $\text{CO}$ , and  $\text{CO}_2$  in Auto Exhaust." Prepared by Philco-Ford Corporation for EPA under Contract No. 68-02-0587. EPA Report No. 650/2-73-030, October 1973.
  2. Burch, D. E., and D. A. Gryvna. "Infrared Gas Filter Correlation Instrument for In-Situ Measurement of Gaseous Pollutants." Prepared by Philco-Ford Corporation for EPA under Contract No. 68-02-0575. EPA Report No. EPA-650/2-74-094. Also, Burch, D. E., and D. A. Gryvna. "Cross-Stack Measurement of Pollutant Concentrations Using Gas-Cell Correlation Spectroscopy." Chapter 10 of Analytical Methods Applied to Air Pollution Measurements, Stevens, R. K. and W. F. Herget, (eds.). Ann Arbor, Ann Arbor Science Publishers, Inc., 1974.
  3. Burch, D. E. "Adjustable Bandpass Filter Employing a Prism." Appl. Opt. **8**, 649 (1969).

The original objective of the project reported here was to incorporate a similar grating assembly in a gas-filter correlation instrument with a multiple-pass sample cell to measure the concentration of formaldehyde in automotive exhaust. This method of measurement promises to be much simpler, and possibly more accurate, than other methods being used for formaldehyde. After the initial phases of the design, it was decided to maintain the same basic instrument with good performance for formaldehyde while making it adjustable with several interchangeable parts so that other gas species could also be studied.

## SECTION II

### SUMMARY

A gas-filter correlation instrument has been built with interchangeable sources, detectors, windows, lenses, gratings and filters for use from approximately 0.3  $\mu\text{m}$  to 11  $\mu\text{m}$ . A precision screw can rotate the grating to the desired orientation to select the center of the spectral band passed by the instrument. Interchangeable slits make it possible to select the width of a single spectral band or of a series of narrow spectral intervals. Spectral curves of transmittance can be scanned by rotating the grating continuously.

The main sample cell has a base length of 1 meter and contains a multiple-pass optical system that can be adjusted to give path lengths up to more than 40 meters. Electrical heating wire coiled around the body of the cell makes it possible to heat the cell to approximately 55°C to avoid condensation of H<sub>2</sub>O. A temperature controller automatically maintains the temperature at the selected level.

The instrument has been equipped with components optimized for the 3.6  $\mu\text{m}$  region where there is strong absorption by formaldehyde, the gas species of primary interest. The majority of the tests were also performed with this gas species in order to obtain good sensitivity and discrimination against other gases, particularly hydrocarbons, that absorb in the same spectral region. The gas-filter cell (GFC) that contains formaldehyde vapor and makes the instrument sensitive to this gas species is heated to approximately 60°C. Powdered paraformaldehyde is placed in the bottom of the cell, and the equilibrium pressure of the formaldehyde vapor over the powder is controlled by regulating the temperature. When all of the instrument parameters are optimized and the sample cell is adjusted to 40 meters path length, the minimum detectable concentration of formaldehyde is less than 0.1 ppm.

Water vapor occurs in relatively high concentrations in automotive exhaust and in many other gas samples that might be analyzed with the instrument. Because of the many H<sub>2</sub>O absorption lines throughout the infrared, this gas is likely to interfere with the measurement of many different gas species. In order to account for possible H<sub>2</sub>O interference, an H<sub>2</sub>O monitor is included in the instrument. The output of the H<sub>2</sub>O monitor can be calibrated to provide an accurate measurement of the H<sub>2</sub>O concentration and can be fed into the main electronics to automatically account for the H<sub>2</sub>O interference.

In addition to the formaldehyde tests, several tests were performed on NH<sub>3</sub> (ammonia) and on vinyl chloride in the spectral region between 10  $\mu\text{m}$  and 11  $\mu\text{m}$  where both of these gas species have very strong absorption features. By

employing spectral intervals only a few  $\text{cm}^{-1}$  wide, it is possible to obtain adequate discrimination against other gases that may be present in the samples. The minimum detectable concentrations are approximately 0.4 ppm for  $\text{NH}_3$  and 1 ppm for vinyl chloride. By obtaining a detector with a smaller sensitive element and a higher detectivity, these values could be reduced by a factor of 5 or more. Additional improvements could also be made by using mirrors with extra high reflectivity and by making other changes to increase the amount of energy transmitted through the optical system.

In the visible and ultraviolet, the performance is limited by low reflectivities of the mirrors and low efficiency of the grating. With the grating, the deuterium-arc lamp source and the photomultiplier provided, the lowest useful wavelength is approximately  $0.32 \mu\text{m}$ . This limit could be extended to shorter wavelengths by employing a grating blazed for shorter wavelengths and mirrors coated for high reflectivity in this spectral interval.

## SECTION III

### CONCLUSIONS

The versatility and high sensitivity of the instrument have been demonstrated. It can operate in the normal mode as a gas-filter correlation instrument with the spectral bandpass being held constant. Gas-filter cells can be interchanged to make the instrument sensitive to virtually any gas that contains sharp absorption features in its infrared, visible, or ultraviolet spectrum. The spectral bandpass can easily be selected to include the absorption features of the gas species to be detected.

The sensitivity, stability and discrimination of the instrument are adequate for most purposes when measuring the concentration of formaldehyde vapor in automotive exhaust. The optimum spectral bandpass and pressure of the formaldehyde vapor in the gas-filter cell have been determined experimentally. Tests performed with ammonia and vinyl chloride indicate that either of these gas species can be measured at low concentrations by gas-filter correlation methods.

By rotating the grating at constant speed, it is possible to scan spectral curves of transmittance. The liquid-nitrogen-cooled detectors provide high enough detectivity that good signal-to-noise ratios can be obtained with the spectral slitwidths as narrow as approximately  $0.5 \text{ cm}^{-1}$  throughout the region between  $3 \text{ }\mu\text{m}$  and  $11 \text{ }\mu\text{m}$ .

Because of the high versatility desired for the instrument, it is necessarily more complex than would be required for a gas-filter correlation instrument designed for a single gas species. In most cases, somewhat better performance could also be attained with an instrument operating on the same basic principles but designed for only one gas species. One factor leading to better performance is the higher reflectivity of the mirrors that would be possible if they were required to operate only over one narrow spectral interval. Several of the optical components could also be made more stable if they were assembled permanently and were not made to be interchangeable.

THIS PAGE LEFT BLANK INTENTIONALLY

## SECTION IV

### RECOMMENDATIONS

The instrument contains two important features that are not found in any other available gas analyzers. One is the versatility that makes it adaptable for the measurement of concentrations of many different gases of interest. The other important feature is its capability for the real-time measurement of the concentration of formaldehyde in automotive exhaust. Maximum value of the instrument can probably be realized by making full use of these two features as opposed to using it for routine measurements that could be performed by other instruments.

Gas-filter correlation techniques have been considered for several gas species for which adequate instruments are not presently available. The instrument reported here can be very valuable in determining the potential performance of any gas-filter correlation instrument that could be designed and built for most gases of interest. Thus, this type of instrument can be evaluated without the cost of building a prototype. The interchangeable and adjustable components make it convenient to determine the optimum spectral bandpass and the optimum amount of gas for the gas-filter cell, and to measure the sensitivity and the interference by gas species other than the one being measured. Different sources of noise and instability can be investigated and related to what might be expected for another instrument designed for a single gas.

Recommended use of the instrument to measure the concentration of formaldehyde is expected to provide valuable information on the overall performance and to indicate possible improvements. Among the items that should be considered are: methods of flushing the sample gas through the sample cell, methods of improving the stability of the "zero-reading", different types of attenuators, methods of controlling the temperature of the formaldehyde gas-filter cell, and alternate methods of mounting the optical components.

THIS PAGE LEFT BLANK INTENTIONALLY

## SECTION V

### LAYOUT AND SPECTROSCOPIC PRINCIPLES

#### OPTICAL COMPONENTS AND LAYOUT

The optical layout of the instrument is illustrated in Figure 1, and Figure 2 is a photograph taken from above and in front of the instrument. Except for a power supply and a few minor accessories, all of the components of the instrument are mounted to a single baseplate of extruded aluminum approximately 38 cm wide by 180 cm long. The optical components consist of five main sections. The mirrors in each section are indicated by an identifying letter as follows: N, entrance section, C, sample cell; X, exit section; G, grating section; and A, alternator. In order to simplify the diagram, the central ray is not included in the sample cell and grating sections. The positions of the extreme rays on the mirror surfaces are indicated, and the images of the source are formed at the places where the extreme rays cross.

The entrance optics contain the radiation source, a 360 Hz chopper and the mirrors that direct the radiant energy into the sample cell. The primary source is a Nernst glower, and alternate sources can be used by placing removable mirror N5 in the position indicated. The long sample cell used to measure formaldehyde concentrations, and other gases of low concentration, has a base-length of one meter and a multiple-pass optical system that can be adjusted to produce pathlengths of more than 40 meters. This sample cell (described in detail in Section VII) has a stainless steel body with inside diameter of 10.2 cm. The sample gas can be left in the cell without flushing, or it can flow continuously in one end of the cell and out the other. The cell can also be evacuated.

The exit section of the instrument consists of the mirrors and other components that direct the beam coming from the sample cell to the entrance slit of the grating section. The grating section provides a means of obtaining essentially any desired spectral interval from approximately 3000 angstroms in the uv to 12 microns in the infrared. The center of the spectral interval passed by the grating section is determined by rotating the grating with a precision screw mechanism. The width of the spectral bandpass is adjusted by varying the opening in a grid, not shown, between two flat mirrors G4 and G5. These two mirrors are mounted perpendicular to each other with the plane of each  $45^{\circ}$  from the horizontal. Energy in the spectral interval passed by the grid is reflected by mirror G5 back to mirror G3. The beam is then returned to the grating, which undisperses it and directs it back to G2 and out the exit slit S2. The emerging beam passes just below mirror G1 before it reaches slit S2. The retro-reflector-grid assembly that contains mirrors G4 and G5 is discussed in greater detail in Section VIII.

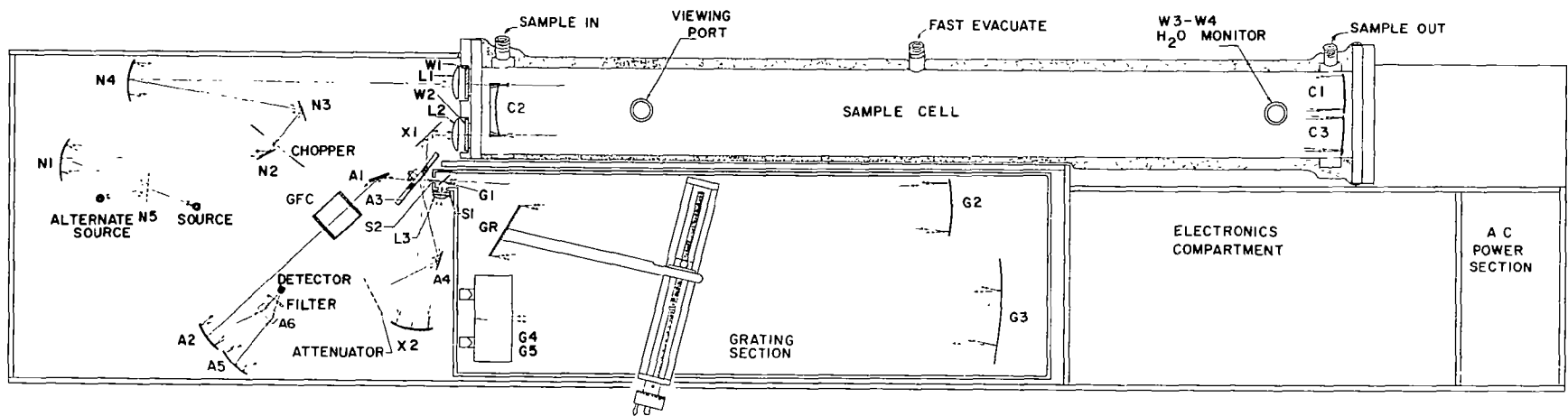


Figure 1. Optical diagram and layout of the instrument.

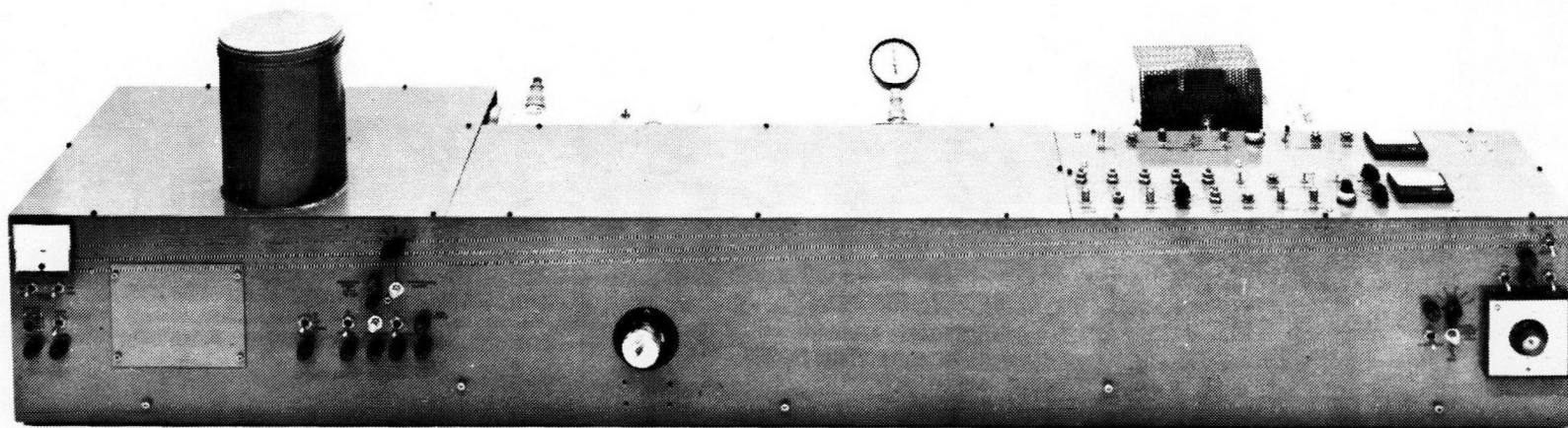


Figure 2. Photograph of the instrument.

The alternator section directs the energy of the selected spectral interval from the exit slit of the grating section to the detector. A rotating mirror chopper, A3, causes the beam to alternately travel over two different paths to the detector. When mirror A3 is in the open position, the energy passes by it to flat mirror A1 and on through the gas-filter cell (GFC) to spherical mirror A2. Flat mirror A6 is tilted  $45^\circ$  from the vertical so that the beam reflected by it is directed upward through a bandpass filter to the sensitive element of the detector. The relative positions of mirror A6, the filter, and the detector have been modified in the diagram so that they can be shown more easily. When mirror A3 is in the closed position, it reflects the beam to mirror A4, through an attenuator, and on to the filter and detector via mirrors A5 and A6. The attenuator is adjusted to provide the same average transmittance over the spectral interval of interest in the attenuator leg as that in the GFC leg. This adjustment is made when there is no sample, or other absorbing gas, in the sample cell. Under this condition, the amount of energy from the source that reaches the detector is the same during each of the halves of the alternator cycle that correspond to the open and closed position of the rotating mirror chopper A3. As discussed in more detail below, the addition of sample to the sample cell modifies the spectral distribution of the transmitted energy in such a way that more energy reaches the detector during the GFC half of the cycle (when the energy is passing through the GFC) than when the energy is directed through the attenuator. This difference results in a modulation of the 360 Hz signal; the frequency of the modulation, 30 Hz, is that of the rotating mirror chopper A3.

The narrow bandpass filter located just below the detector serves two important purposes. First, it blocks out radiant energy of overlapping orders that are transmitted by the grating section. For example, if the grating section is adjusted to pass through  $3.6 \mu\text{m}$  energy, it also passes  $3.6/2$ ,  $3.6/3$ ,  $3.6/4 \mu\text{m}$ ... etc. The narrow bandpass filter passes the  $3.6 \mu\text{m}$  energy and blocks the overlapping orders of shorter wavelengths. It can also be used to pass second or third order while blocking out all others. Another important function of the bandpass filter is to reduce stray energy that may reach the detector. This scattered light may originate from several different places. One possibility is energy from the source that is chopped at 360 Hz by the high frequency chopper and is scattered from various components to the detector via paths other than the desired one. This energy is undispersed and therefore covers a wide spectral interval. Much of it is eliminated by shields not shown in the figure, but it is further reduced by the narrow bandpass filter.

The rotating mirror chopper, A3, emits some energy and reflects other energy emitted by the GFC or other components to the detector. This energy is modulated at the alternator frequency, 30 Hz, because of the rotation of mirror A3. This energy results from temperature gradients between different components in the instrument. This modulated energy is not dispersed by the grating section and covers a wide spectral interval. Therefore, it is greatly reduced by the narrow bandpass filter in front of the detector. Energy that is not modulated does not degrade the performance of the instrument. To a large extent, the 30 Hz energy emitted or reflected by mirror A3 is not chopped at 360 Hz and is accounted for by the electronics used to process the detector signal. However, if this 30 Hz signal is too large, it can saturate some of the electronic components, or the harmonics of the signal can be transmitted to produce errors in the measurements.

Two additional measurable quantities are defined as follows:

$$\bar{T}_{g,s} = \frac{\int M N_{\nu} R T_f T_g T_s d\nu}{\int M N_{\nu} R T_f T_g d\nu} = \frac{E_g}{E_g^0}, \quad (6)$$

$$\bar{T}_{at,s} = \frac{\int M N_{\nu} R T_f T_{at} T_s d\nu}{\int M N_{\nu} R T_f T_{at} d\nu} = \frac{E_{at}}{E_{at}^0}. \quad (7)$$

The quantity  $\bar{T}_{g,s}$  in Equation (6) is the average transmittance of a sample as it would be measured in the beam that also passes through the GFC. Similarly, Equation (7) gives the average transmittance of a sample as it would be measured in the beam that passes through the attenuator side of the alternator. In most situations, the attenuator transmittance  $T_{at}$  is essentially constant over the spectral interval being considered; therefore, this factor can be removed from under the integral signs of Equation (7), making this equation identical to Equation (3). Thus,  $\bar{T}_{at,s} = \bar{T}_s$ . The average absorptances that correspond to the average transmittances defined by Equations (6) and (7) are:

$$\bar{A}_{g,s} = 1 - \bar{T}_{g,s}, \text{ and} \quad (8)$$

$$\bar{A}_{at,s} = \bar{A}_s = 1 - \bar{T}_{at,s} = 1 - \bar{T}_s. \quad (9)$$

When the sample contains gas of species x, the same species as in the GFC, there is a positive correlation between the spectrum of the sample ( $T_g$ ) and the spectrum of the GFC ( $T_g$ ). Because of this positive correlation in the spectral structures,  $\bar{T}_{g,s}$  is greater than  $\bar{T}_s$ , and  $E_g$  is greater than  $E_{at}$ . A sample may contain gas other than species x that absorbs in the spectral interval passed by the instrument (where  $T_f \neq 0$ ). If the spectral structure of such a gas has no correlation with the spectral structure of species x,  $\bar{T}_{g,s} = \bar{T}_{at,s}$ , and  $E_g = E_{at}$ . In the case that the spectral structure of the sample gas is such that  $E_g < E_{at}$ , and  $\bar{T}_{g,s} < \bar{T}_{at,s}$ , there is said to be negative correlation between the sample gas and species x. It follows that a gas species in the sample that is negatively correlated with species x will cause the instrument to indicate too low a concentration of species x, the species being measured.

We define two additional useful quantities:

$$\Delta = E_g - E_{at}, \quad (10)$$

$$\Sigma = E_g + E_{at}. \quad (11)$$

The quantity  $\Delta$  represents the difference in the chopped energy reaching the detector during the two halves of the alternator cycle and is therefore proportional to  $V_a$ , the 30 Hz component of the detector signal. The constant factor relating  $V_a$  to  $\Delta$  depends on the gain of the system between the detector and the point where  $V_a$  is measured. Similarly,  $\Sigma$  is the sum of the same two energy values and is proportional to the average value of  $V_c$ , the 360 Hz component of the amplified detector signal. The voltage  $V_a$  is zero for no sample and is directly related to the concentration of the gas species in the sample cell. From Equations (1), (2), and (10), we see that  $\Delta$  and  $V_a$  are also proportional to the spectral radiance  $N_\nu$  of the source and to the responsivity  $R$  of the detector. Thus, if the electronic gain remains constant, calibration data relating  $V_a$  to concentrations are valid only as long as  $N_\nu$  and  $R$  also remain constant. Changes in  $N_\nu$  and  $R$  also influence  $\Sigma$  by approximately the same factor as they do  $\Delta$ . Therefore, the ratio  $\Delta/\Sigma$  is independent of changes in either  $N_\nu$  or  $R$  as long as either changes by a constant factor over the spectral interval of interest. Neither  $\Delta$  nor  $\Sigma$  is easy to measure directly; however, the ratio  $\Delta/\Sigma$ , which is proportional to  $V_a/V_c$ , is measured by the instrument described in this report. In adjusting the instrument gain settings, the radiant energy beam through the attenuator is temporarily blocked so that  $T_{at}$  and, in turn,  $E_{at}$  equal zero. Under this condition,  $\Delta/\Sigma = 1$ , and the amplifier gain settings are adjusted so that the voltages  $V_a$  and  $V_c$  are equal.

We define

$$V' = V_a/V_c \quad (12)$$

with the gain settings adjusted as just described. The gain settings that affect this ratio are kept fixed so that  $V' = V_a/V_c = \Delta/\Sigma$  when the attenuator is unblocked and measurements are made.

An automatic gain control (AGC) circuit maintains  $V_c$  constant to simplify the measurements. When this is used,  $V'$  is proportional to  $V_a$ , a quantity that is measured directly by the instrument. Thus, only one voltage,  $V_a$ , needs to be read in order to determine  $\Delta/\Sigma$ , the quantity that is related directly to the absorber thickness of the gas species being measured. Calibration data are obtained by measuring  $V'$  for a series of standard samples of known concentration.

In practice, small changes in the average  $N_\nu$  due to variations in source temperature are also accompanied by second order changes in the spectral distribution. These slight changes can cause small differences in  $E_g^0$  and  $E_{at}^0$  if there is any correlation between  $N_\nu$  and  $T_g$ . This results in a slight shift to the "zero" that is measured with no sample. After a few hours warm-up time for the instrument, zero-shifts due to source or detector variations over periods of several minutes usually correspond to changes in  $V'$  of less than  $10^{-4}$ , which corresponds approximately to the lowest concentrations being measured. These small shifts can be determined and accounted for easily by flushing the sample cell with a non-absorbing gas. Ordinary changes in  $N_\nu$  and  $R$  do not significantly affect the relationship between absorber thickness and  $V'$ , if the small zero shift is accounted for.

The accumulation of dirt on mirrors or windows can reduce the energy reaching the detector. If the dirty components occur outside of the alternator section, the attenuation affects both  $E_g$  and  $E_{at}$  by exactly the same factor, provided the attenuation is the same over the entire spectral interval of interest. Thus,  $\Delta/\Sigma$  and  $V'$  are unaffected by the dirt as long as enough energy reaches the detector to make the AGC operate properly. Thus, the system involving the two frequencies,  $f_c$  and  $f_a$ , along with the AGC circuits provides a reliable and convenient method of determining concentration from a single voltage measurement.

In considering the effect of dirt on windows, or of anything else that may obstruct part of the radiant energy beam, it becomes apparent that none of the components in either leg of the alternator should provide an aperture stop or limit the field-of-view. This corresponds to a different value of  $M$  in Equation (1) than in Equation (2). If they are different, an obstruction to part of the beam anywhere outside of the alternator might have a different effect on the beam through one leg of the alternator than on the beam through the other leg. For example, let us consider the case in which the windows on the GFC are too small to accept all of the beam incident upon them, but the attenuator leg transmits the entire beam. An obstruction in the beam that blocks rays that would be blocked by the undersize GFC windows would not reduce  $E_g$ , but it would reduce  $E_{at}$ . This would result in a zero-shift of the instrument. The seriousness of this type of situation depends on how frequently and how easily a "zero-reading" can be made with no absorbing gas in the sample cell.

An aperture stop or a limit to the field-of-view in either leg of the alternator can also reduce stability, which may be a more important consideration than a slow change in the zero reading such as the one discussed in the previous paragraph. Consider a "geometrical" attenuator that completely blocks a portion of the edge of the beam in the attenuator-leg of the alternator. A slight displacement of the beam will cause the attenuator to block a different fraction of the beam with a resulting change in  $E_{at}$ . Since the instrument measures a small difference,  $\Delta$ , between two relatively large signals,  $E_g$  and  $E_{at}$ , it is naturally quite sensitive to small changes in  $E_{at}$ , that are not accompanied by a corresponding change in  $E_g$ . Beam displacements that produce this kind of instability can result from slight shifts in many of the different optical components, particularly from wobble in the rotating mirror chopper. When good instrument stability is required so that small values of  $V'$  can be measured, it is best to employ neutral density attenuators that have the same transmittance over all of the area covered by the radiant energy beam.

In some cases, it is difficult to obtain neutral density attenuators with the proper  $T_{at}$ , and a geometrical-type attenuator provides the simplest method of obtaining a balance between  $E_g^o$  and  $E_{at}^o$ . The attenuator illustrated schematically in Figure 1 contains two parts, an interchangeable neutral density part and a geometrical type that can be used when needed. In order to reduce the instability and noise produced by the geometrical attenuator, it is made so that it attenuates near the center of the beam, rather than at an edge of the beam. The flat, blade-like attenuator extends horizontally across the entire center portion of the beam where the illumination is very nearly uniform. Thus, small displacements of the beam produce only very small changes in  $T_{at}$ . The amount of attenuation is adjusted by rotating the thin blade about its axis along the length of the blade. Noise on the output,  $V'$ , produced by this geometrical attenuator can be kept to no more than about  $10^{-5}$ , which is much less

than we have been able to attain with combs or with attenuators that block the edge of the beam.

The correlation efficiency  $C_e$  is defined as

$$C_e = \frac{\bar{A}_{at,s} - \bar{A}_{g,s}}{\bar{A}_{at,s}} = \frac{\bar{T}_{g,s} - \bar{T}_{at,s}}{1 - \bar{T}_{at,s}} \quad (13)$$

Consider the ideally correlated system in which the GFC is completely opaque at all wavenumbers where there is any absorption by the sample. In terms of the above quantities, this can be stated as  $T_g = 0$  if  $T_s \neq 1$  and  $T_f \neq 0$ . By applying this condition to Equations (1) and (6), we see that  $E_g$  is unaffected by the addition of the sample and that  $\bar{T}_{g,s} = 1$ . ( $\bar{A}_{g,s} = 0$ ). In this idealized system, we see that  $C_e = 1$ , the maximum value possible for a system employing an attenuator with  $T_{at}$  constant for all wavenumbers. It can be seen that  $C_e$  would be greater than 1 if the attenuator had spectral features that were negatively correlated with the sample gas. This specialized case is not applicable to the instrument described here and is not discussed further.

The correlation efficiency is an important parameter that is quite useful in describing the performance of a GFC instrument. It is related to the spectral structure of the gas species being measured but not to the intensity of the absorption. If  $C_e$  is between approximately 0.7 and 1, the correlation is quite good, and it is likely that the instrument can be made to operate with good sensitivity and good discrimination against other gases that might absorb in the same spectral region. Good performance for many applications can also be attained with instruments with lower correlation efficiency. Carbon monoxide is an example of a gas with spectral structure that is well suited to GFC techniques; the spectral lines are well separated, narrow and of about uniform intensity over intervals several  $\text{cm}^{-1}$  wide. We have designed and built CO instruments with  $C_e > 0.9$ . On the other hand, much lower values of  $C_e$  are expected for gases whose spectral structure is not "sharp" but contains portions with intermediate absorption that is strong enough to be significant but weaker than the strongest absorption in the interval. Reference 2 discusses the  $\text{SO}_2$  absorption near 4  $\mu\text{m}$ , which is a good example of spectral structure with a low correlation efficiency.

With the instrument described in this report, either of the quantities  $\bar{T}_{g,s}$  or  $\bar{T}_{at,s}$  can be measured directly by blocking the attenuator leg or the GFC leg of the alternator, respectively. The ratio of the carrier voltages  $V_c$  measured with and without the sample gives the values of either  $\bar{T}_{g,s}$  or  $\bar{T}_{at,s}$  depending on which leg of the alternator is being used. From these two quantities, the value of  $C_e$  can be determined by the use of Equation (13). The value of  $C_e$  will, in most cases, depend slightly on the amount of the sample gas. Of most interest is the value for samples of low concentration for which  $\bar{A}_{at,s}$  and  $\bar{A}_{g,s}$  are  $\ll 1$ .

Values of  $C_e$  can also be determined from measurements of  $V'$  and  $\bar{A}_{at,s}$ . This method of measuring  $C_e$  has certain advantages when the sample absorbance is proportional to  $V'$  and is measured directly. For  $\bar{A}_{at,s} \ll 1$ , we can show that

$$V' = \frac{\Delta}{\Sigma} = \frac{\bar{A}_{at,s} - \bar{A}_{g,s}}{2}, \text{ and} \quad (14)$$

$$C_e = \frac{2 V'}{\bar{A}_{at,s}} \quad (15)$$

Values of  $C_e$  can also be determined from measurements of  $V'$  along with  $\bar{A}_{g,s}$ , or from  $V'$  along with measurements of the uncontrolled carrier voltage  $V_c$  as a sample is added and removed. In the latter case,  $V_c$  is proportional to  $E_g + E_{at}$ , and the apparent absorptance,  $\bar{A}_{g+at,s}$  of the sample measured with the combination of the attenuator and GFC is

$$\bar{A}_{g+at,s} \cong \frac{\bar{A}_{at,s} + \bar{A}_{g,s}}{2}. \quad (16)$$

If  $\bar{A}_{at,s} \ll 1$ , ( $\bar{T}_{at,s} \cong 1 \cong \bar{T}_{g,s}$ ), it follows that

$$V' = \bar{A}_{at,s} - \bar{A}_{g+at,s}. \quad (17)$$

The instrument described in this report is particularly well suited for the simultaneous measurements of  $V'$  and  $\bar{A}_{g+at,s}$ . Thus  $C_e$  can be determined easily for different GFC parameters and different bandpasses by the use of Equations (15), (16), and (17). Many of the data discussed in later sections of this report were obtained in this manner.

For samples at the same total pressure, the absorption is a function of the sample absorber thickness  $u$  given by

$$u \text{ (atm cm)} = p \text{ (atm)} \ell \text{ (cm)} = 10^{-6} c \text{ (ppm)} P \text{ (atm)} \ell \text{ (cm)}, \quad (18)$$

where  $p$  is the partial pressure of the absorbing gas and  $c$  is its concentration in parts per million volume.  $P$  is the total pressure and  $\ell$  is the geometrical length of the optical path through the sample. By this definition, 1 atm cm is equivalent to  $10^4$  ppm meters. In some investigations dealing with samples covering a wide temperature range, the absorber thickness is defined differently in order to account for the change in density at different temperatures. This difference in definition must be taken into account when comparing results of different workers.

Another very useful parameter in describing instrument performance that depends on both  $C_e$  and the intensity of the absorption is

$$F = \lim_{u \rightarrow 0} \left[ \frac{V'}{u} \right] \text{ (atm cm)}^{-1}. \quad (19)$$

This quantity has been named the Pembroke factor for John Pembroke, one of our colleagues, who has done extensive work in evaluating GFC instruments.

It follows from Equations (14) and (18) that for  $u$  sufficiently small that  $A_s \ll 1$  for all wavenumbers of interest,

$$F = \frac{C_e \bar{A}_{at,s}}{2u} . \quad (20)$$

We define another measurable quantity

$$\bar{k}_s = \frac{-\ln \bar{T}_{at,s}}{u} \text{ (atm cm)}^{-1} . \quad (21)$$

This average absorption coefficient  $\bar{k}_s$  can be measured without a GFC instrument and is related directly to the intensity of absorption by the gas; it is nearly independent of  $u$  as long as  $-\ln \bar{T}_{at,s} \ll 1$ . Under this condition,  $-\ln \bar{T}_{at,s} = \bar{A}_{at,s}$ , and

$$F = \frac{C_e \bar{k}_s}{2} \text{ (for } \bar{A}_{at,s} \ll 1) . \quad (22)$$

## SECTION VI

### FORMALDEHYDE GAS-FILTER CELL

The formaldehyde gas-filter cell acts as a selective filter for the detection of formaldehyde and is located in the position indicated by GFC in Figure 1. The GFC for formaldehyde is necessarily more complicated than it is for many other gases because of the low vapor pressure of formaldehyde near room temperature. Paraformaldehyde powder is placed in the GFC, and the pressure of the formaldehyde vapor above the powder is controlled by controlling the cell temperature.

The construction of the formaldehyde GFC is illustrated in Figure 3. The body of the cell is made of stainless steel, and the optical path through the cell is approximately 5 cm. Electrical resistance wire heats the cell, which is covered with asbestos insulation in order to reduce the amount of heat dissipated to the remainder of the instrument. The right-hand portion of Figure 3 shows a sectional view of the main body of the cell; the left-hand portion of the figure is divided into three parts. The right-hand part is a sectional view, and the center-section is a drawing of a part of the cell body without the insulation in place. Insulation is shown in place in the left-hand portion of the figure. Heating wire that is coiled around the body of the cell is not included in the figure. The bottom plate of the cell is sealed to the main body with a Teflon O-ring and can be removed in order to add more paraformaldehyde powder. Four fiber blocks, each approximately 1.2 cm long and 1.2 cm in diameter, support the cell and insulate it from the main baseplate of the instrument.

Cell pressures can be measured with a pressure transducer mounted directly to the main cell body and insulated to keep its temperature close to the remainder of the cell. A small valve, which is also insulated, makes it possible to evacuate the cell or to add nitrogen or any other gas that may be desired. Two sapphire windows are used on each end; one provides a vacuum tight seal, and the outer one provides thermal insulation for the inner window, which is in contact with the formaldehyde vapor. The windows are approximately 42 mm in diameter and 1.5 mm thick.

The heating coils and insulation are designed to maintain a temperature gradient such that the inner window on each end is a few degrees centigrade above the remainder of the cell in order to avoid condensation of formaldehyde on the window. A small amount of paraformaldehyde powder is placed in the inside of the bottom plate, the coolest part in contact with the formaldehyde vapor. Thus, the pressure of the vapor is expected to be approximately equal to the vapor pressure of the powder at the temperature of the bottom plate. Most of the heat

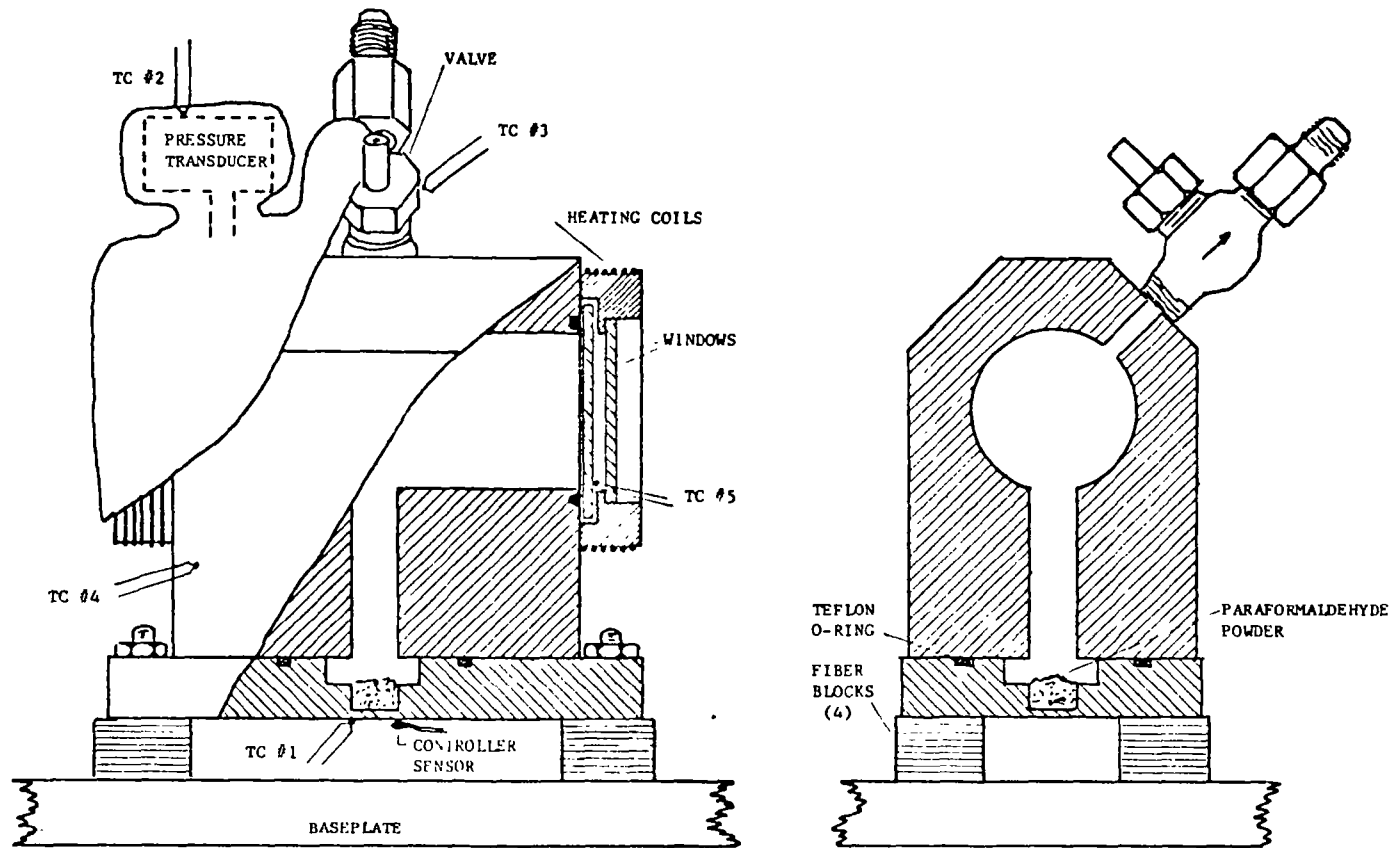


Figure 3. Two drawings of the formaldehyde gas-filter cell.

is provided by heating wire coiled around the outside edge of the window holders. Some additional heat is provided by heating wire wrapped around the valve and the pressure transducer to maintain these parts at approximately the same temperature as the main body of the cell. The asbestos insulation, which is approximately 1 cm thick, around the body of the cell reduces the amount of heat loss through the walls of the cell. A large portion of the heat flow is from the heating coils through the body of the cell and the bottom plate to the main baseplate of the instrument. By experimenting, we found that the four fiber supporting blocks provide about the optimum amount of insulation between the cell and the main baseplate. With more insulation, there is not enough heat flow through the cell to maintain the temperature of the baseplate sufficiently far below the window temperature to avoid condensation on the windows. Small aluminum blocks, which were tried in the place of the fiber blocks, did not provide enough thermal insulation and required much more heat in order to maintain the lower plate of the cell at the desired temperature.

The window holders are circular with insulated resistance wire placed in threads around the outside surface. The inner window of each end is pressed against a Teflon O-ring to provide a good vacuum seal. The metal ring that holds the window makes metal-to-metal contact with the body of the cell, and the Teflon O-ring keeps the sapphire window from contacting the metal cell body. This type of construction allows the parts to expand differently as the cell is heated or cooled while maintaining the vacuum seal. The metal surface of the cell body does not need to be machined as flat as if it were in direct contact with the sapphire window. Slight irregularities in the metal would cause the window to break as pressure was applied to it if the metal and the window were in contact. The dead air space between the outer and inner windows provides insulation so that the window in contact with the formaldehyde vapor is not cooled by the air. The outer window is held in place by a silicone rubber cement.

An adjustable temperature controller maintains the temperature of the GFC at any desired level between approximately 40°C and 75°C. The sensor for the controller is attached to the bottom plate of the GFC near the paraformaldehyde powder as indicated in Figure 3. The controlling unit is mounted on the underneath side of the main baseplate and is accessible for adjustment from the end of the instrument near the source. A transformer used in conjunction with the controller limits the maximum voltage applied to the heating coils to approximately 30 Volts. The power is turned on and off with a period of approximately two seconds. The fraction of each period that the power is applied is proportional to the error signal, the difference between the sensor temperature and the control temperature to which the controller is adjusted. When the cell is being heated initially, or when the control temperature is changed, the cell temperature will stabilize with an insignificant amount of oscillation of the temperature. When the GFC temperature is changed, the pressure of the formaldehyde vapor also changes, but as much as two days may be required for the vapor pressure to stabilize after the temperatures have come to equilibrium.

The temperature of the GFC can be monitored at five key points by thermocouple junctions that have been bonded to the cell in the positions indicated in Figure 3. One of these thermocouple junctions monitors the temperature on the bottom plate adjacent to the sensor for the controlling unit and provides a check on the consistency of the controller. Thermocouple junctions are also placed on the pressure transducer and on the valve in order to be sure that sufficient heat is

being applied to these parts to maintain them at approximately the same temperature as the cell body. The fourth thermocouple junction is embedded in the main body of the cell and measures the average temperature of the vapor. Leads from the thermocouple junctions go to a five-position switch mounted on the front panel of the instrument. The switch connects any one of the five thermocouples to a BNC connector also mounted on the front panel. A vacuum voltmeter, or other d.c. voltmeter with high input impedance, can be connected to the BNC fitting to monitor the temperature at any one of the five thermocouple locations. The voltmeter reading is proportional to the difference between the temperature of the thermocouple junction and the temperature of the switch, which is normally not more than 1 or 2 degrees centigrade above room temperature.

The relationship between the pressure of the formaldehyde vapor and the GFC temperature is shown graphically in Figure 4. The data were obtained by monitoring the pressure with the pressure transducer for different cell temperatures indicated by thermocouple No. 1, which measures the temperature of the coolest point in contact with the formaldehyde vapor. The pressures were measured after the temperature had been stabilized for several hours; however, in some cases the pressure may have not reached equilibrium. Pressures obtained from Figure 4 may be in error by as much as 10 or 15%, but they are sufficiently accurate to determine if the cell is operating properly. If more accurate values were required, it would probably be necessary to employ a more sensitive pressure transducer and to check its calibration at the different temperatures employed. More time would also be required in order to ensure that the vapor pressure had reached equilibrium for each temperature.

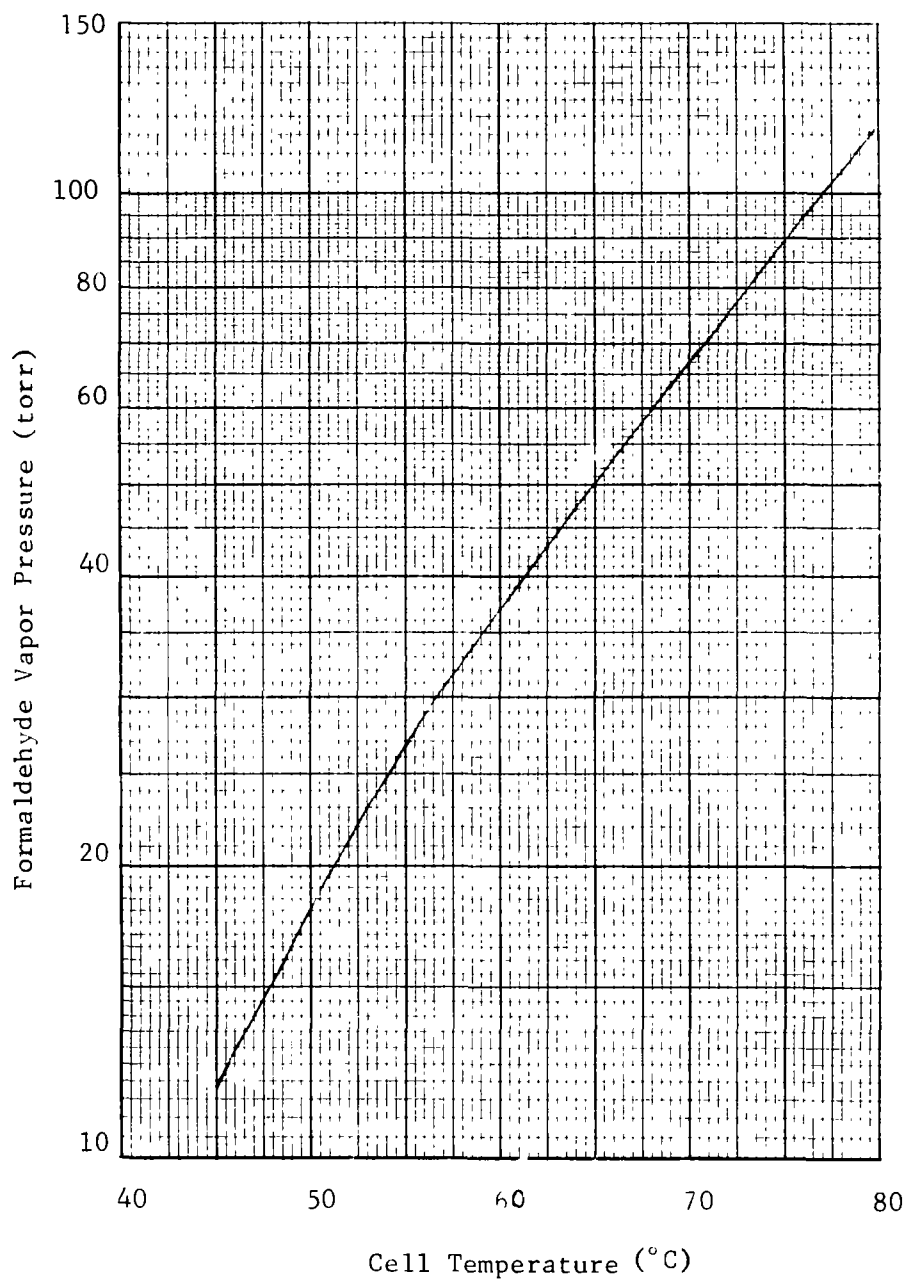


Figure 4. Plot of the pressure of formaldehyde vapor vs the GFC temperature. The temperature corresponds to the coldest spot in contact with the formaldehyde vapor.

THIS PAGE LEFT BLANK INTENTIONALLY

## SECTION VII

### MULTIPLE-PASS SAMPLE CELL

#### OPTICAL AND MECHANICAL

A view of one end of the multiple-pass sample cell from the back side of the instrument is shown in Figure 5. The cell is supported by two V-shaped fiberglass blocks that insulate it from the main baseplate. A portion of one of the fiberglass blocks can be seen in Figure 5. Adjustable metal straps hold the cell down against the blocks. A stainless steel tab welded to the underneath side of the cell body and bolted to the block nearest the window end of the cell holds the cell in the proper position. The cell body can slip endwise relative to the other fiberglass block to account for expansion when the cell is heated. The transmitting optics of the H<sub>2</sub>O monitor seen on the top of the cell are discussed in Section X.

Figure 6 illustrates the manner by which the gas enters the sample cell. Eight small holes drilled through the wall of the sample cell are covered by a hollow ring that is welded in place around the outside of the cell body. The sample gas enters a pipe fitting that is welded into the hollow ring and flows around the inside of the ring to enter the cell through the eight small holes. By introducing the gas through several holes spaced around the cell, turbulence produced by the incoming gas is greatly reduced, and the beam of infrared energy is more stable than it would be if the gas entered through a single large hole.

The opposite end of the cell has a similar arrangement for the gas to exit from the cell. Both ends are essentially identical so that the direction of flow can be reversed. The inlet and exit ports are placed close to the ends in order to reduce the amount of stagnant air in the ends of the cell as the sample flows through. Our tests indicate that with the sample cell adjusted to 40 passes, no serious problem is created by turbulence when the sample is flowing fast enough to flush out essentially all of the sample in one minute. A pipe fitting similar to those used on the inlet and outlet ports is welded directly to the wall of the cell near its center. A vacuum pump connected to this fitting will evacuate the cell more quickly than if the gas were pumped through the small holes in the wall near the inlet or outlet port. If the fitting is not connected to a vacuum pump, it can serve as a fitting for a gauge as shown in Figure 2.

Figure 6 also shows an optical diagram of the bypass optics assembly that can be installed so that the monitoring beam does not enter the multiple-pass sample cell. Operation with the bypass optics in place might be desirable for studies in which a sample cell is no longer than a few centimeters. In this case, the sample cell could be placed in the beam between mirror N4 and the bypass optics assembly. Mirrors B1, B2 and B3 are permanently mounted to a block that fits into position and bolts directly to the main baseplate. Mirror X1, whose normal

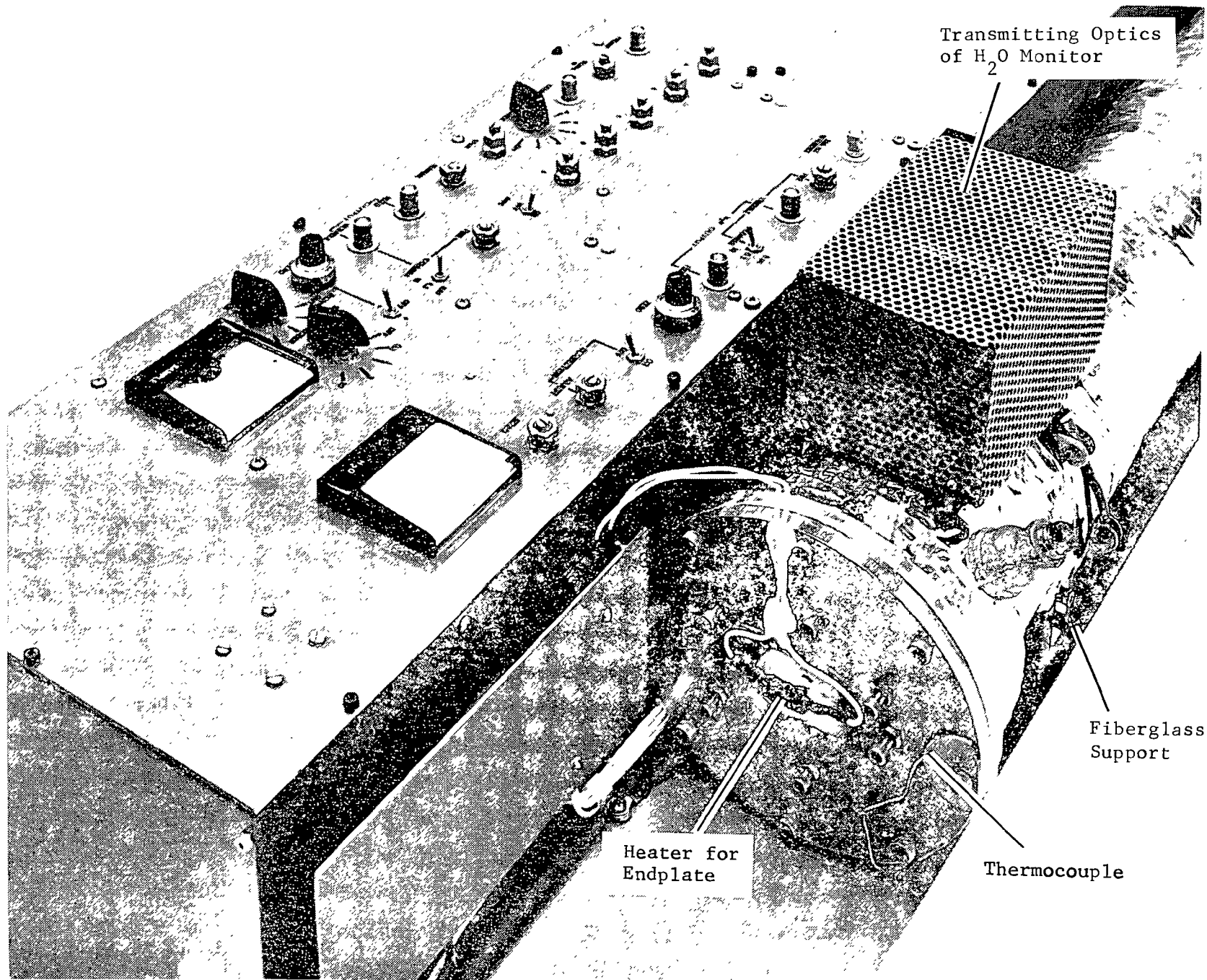


Figure 5. Photographic view of one end of the multiple-pass sample cell from the back side of the instrument.

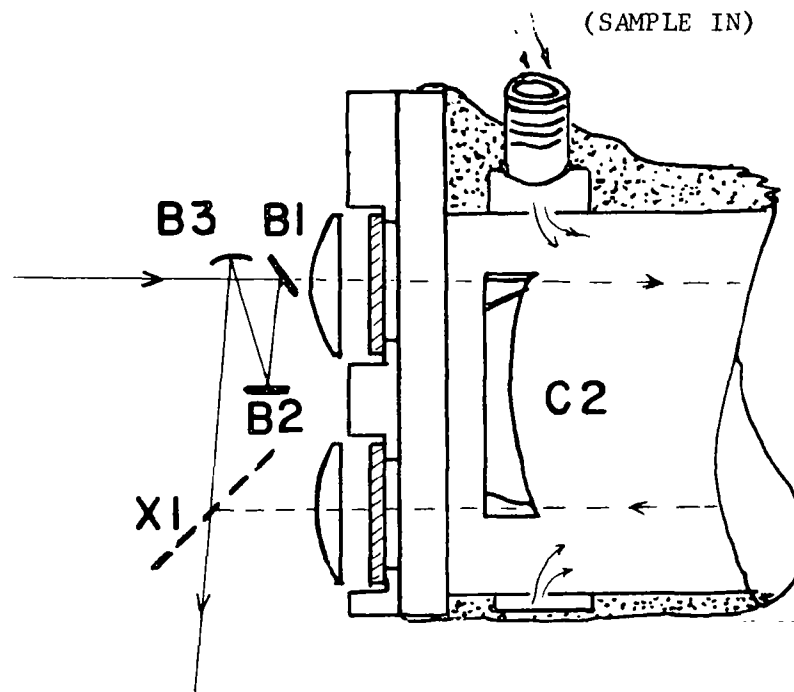


Figure 6. Sample inlet and optical diagram of the bypass optics assembly. Bypass mirrors B1, B2, and B3 are mounted on a block that fits into place when mirror X1 is removed.

position is indicated in Figure 6 by a broken line, is removed before the bypass optics assembly is put in place. Small pins in the baseplate guide the bypass optics assembly so that it can be removed and replaced easily with little alignment necessary.

As indicated in Figure 1, an image of the source is formed inside the multiple-pass sample cell adjacent to mirror C2. As the beam leaves the multiple-pass sample cell, a similar image on the opposite side of C2 acts as a source that is imaged by mirror X2 onto the entrance slit of the grating section. When the bypass optics are in place, the beam that would normally enter the multiple-pass cell is intercepted by mirror B1, and the image of the source is formed near mirror B3. This image then acts as a source that is imaged on the slit of the grating section. Spherical mirror B3 acts as a field mirror and greatly reduces the vignetting that would occur if it were flat.

Two sets of windows are supplied for the multiple-pass sample cell. Sapphire windows 38 mm in diameter and 2 mm thick are used for wavelengths shorter than approximately 5.5  $\mu\text{m}$ . Windows of NaCl are used for longer wavelengths out to approximately 15  $\mu\text{m}$ ; they are not used unless they are required because they are hygroscopic and must not be exposed to humid air over extended periods of time. O-rings not shown in the figures provide a vacuum seal between the windows and the end flange. Metal clamps hold the windows and the field lenses L1 and L2. Field lenses made of  $\text{CaF}_2$  can be used from the ultraviolet to approximately 8  $\mu\text{m}$ ; a set of NaCl lenses are provided for the longer wavelengths. A vacuum seal between the end of the multiple-pass sample cell and the removable end flange is provided by O-ring gaskets made of buna-N rubber.

The optical principles of the multiple-pass sample cell, first described by White,<sup>4</sup> can be explained with the aid of Figure 7. The upper portion of the figure shows mirror C2 as viewed from the opposite end of the multiple-pass cell. Entrance window W1 and exit window W2 are indicated. The large circle corresponds to the 10.2 cm inside diameter of the cell body. The image indicated by the 0 is the one formed near mirror C2 by mirror N4 of the entrance optics (see Figure 1). The beam continuing from this image strikes mirror C1, the center of curvature of which is near the front surface of mirror C2 in the position indicated by an X in the upper portion of Figure 7. Image 0 is at a distance from mirror C1 equal to the radius of curvature of C1; therefore, image No. 2 is formed in the same plane as image 0 with the two images symmetrically placed around X, the center of curvature of mirror C1. Mirror C2 is also spherical, and its center of curvature is between mirrors C1 and C3 so that C2 forms an image of C1 on C3, and vice versa.

Energy from image 2 is reflected to mirror C3, which in turn, forms another image on mirror C2 at the position indicated by 4. Images 2 and 4 are symmetrical about the center of curvature of mirror C3 indicated by the circle adjacent to the X in Figure 7. The beam continues back and forth in this manner

---

4. White, John U. Long Optical Paths of Large Aperture. Journal of the Optical Society of America. 32:285-288, May 1942.

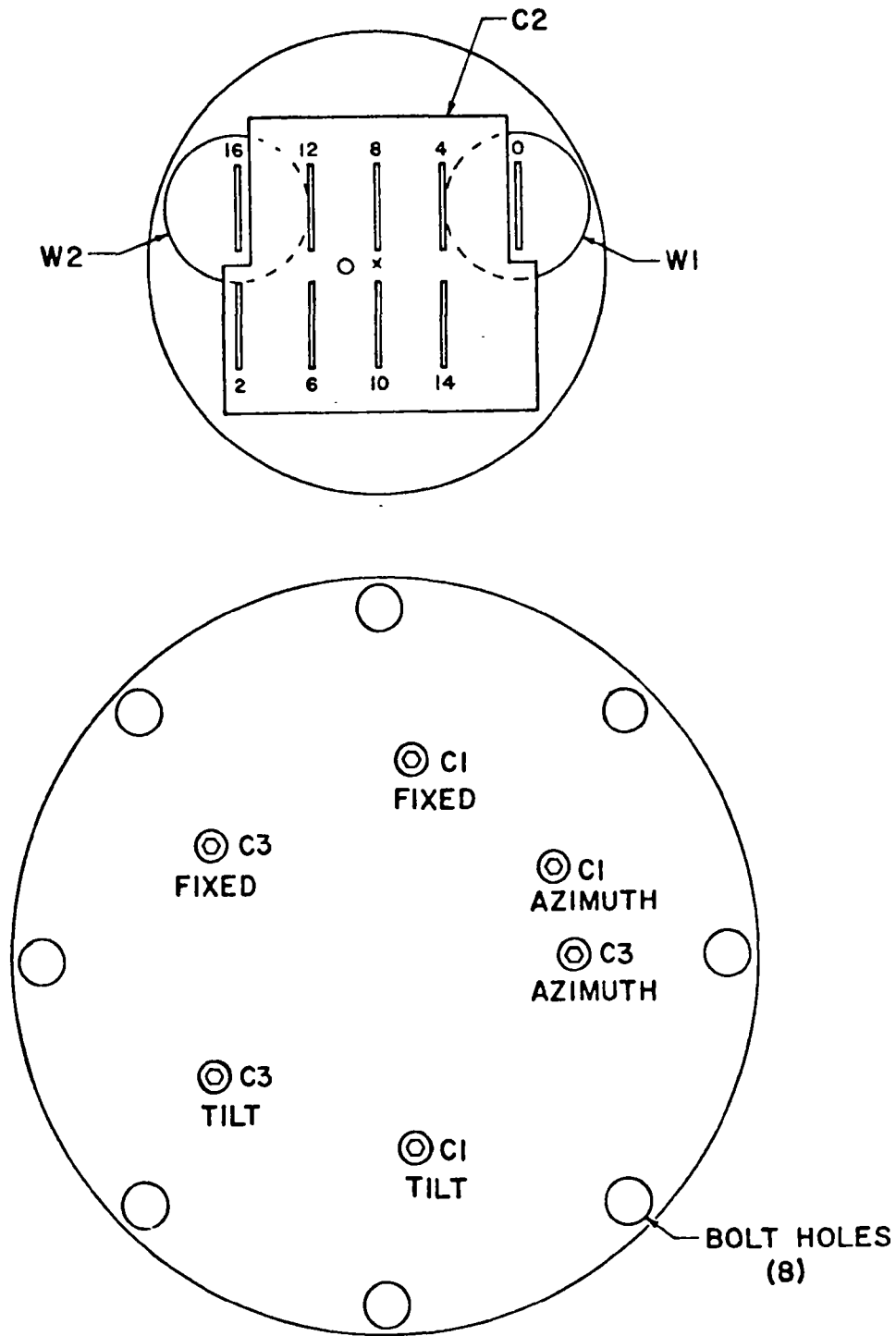


Figure 7. Multiple-pass optical system in the sample cell. The upper portion shows positions of the images on mirror C2 when the cell is adjusted to 16 passes. The positions of the screws used to adjust mirrors C1 and C3 are indicated in the lower portion.

forming images on mirror C2 as shown. The number adjacent to each image indicates the number of passes the beam has made at the time the image is formed. In the arrangement shown, the beam misses mirror C2 after 16 passes and exits through window W2.

After the sample cell is initially adjusted, the position of mirror C1 is left fixed so that it forms image 2 close to the position shown. The number of passes is changed by adjusting the azimuth angle of mirror C3 to move its center of curvature horizontally. When the centers of curvature of mirrors C1 and C3 are close together, the images on mirror C2 are also close together and the beam makes several passes before it emerges through the exit window. After the optical system has been adjusted to give the desired number of passes, a small tilt adjustment of mirror C3 may be required in order to form the exit image at the proper height. After a tilt adjustment has been made, a final azimuthal adjustment may be required because the azimuth adjustment is the most critical.

Mirrors C1 and C3 are adjusted from outside the cell by rotating the screws that pass through the end plate. Jam nuts on the screws lock the screws solidly in place. If the cell is to be used at less than atmospheric pressure and leak-tight seals are required, the screws are potted in silicone rubber after the adjustments are completed.

#### TEMPERATURE CONTROL

Electrical heating wire wrapped around the outside of the cell body makes it possible to heat the cell to any desired temperature up to approximately 55°C. Heating the cell avoids condensation of H<sub>2</sub>O vapor when studying raw automotive exhaust, or any other samples with moderately high concentrations of H<sub>2</sub>O. One piece of heating wire is wrapped around the cylindrical body of the cell with adjacent coils closer together near the ends than in the middle to help account for heat loss from the ends. A power resistor bonded with good thermal contact to each endplate supplies additional heat to the ends so that there is less than 2°C variation in the temperature throughout the length of the cell. Fiberglass insulation with metallic foil coating is wrapped around the cylindrical body and covers the heating wire.

A temperature controller senses the temperature of the cell wall near the center and maintains it at a pre-set level. The dial of the controller can be seen near the right-hand end of the instrument in Figure 2. Five thermocouples sense the temperature of the cell. One is connected to each endplate, and the other three are connected to the cell wall, near the center and approximately 25 cm from each end. A five-position switch connects each thermocouple to a BNC fitting on the front panel where it can be coupled easily to a voltmeter to measure the temperature at any of the five positions.

## SECTION VIII

### GRATING SECTION

The grating section acts as a conveniently adjustable bandpass filter that can provide virtually any desired spectral bandpass from approximately  $0.3 \mu\text{m}$  to more than  $11 \mu\text{m}$ . The beam of radiant energy enters the grating section through the entrance slit S1 on which an image of the source is formed. A wide selection of slits are available, ranging in width from approximately 0.1 mm to 2.4 mm. The slits are cut by a laser in small pieces of stainless steel shimstock, approximately 0.08 mm thick by 0.95 cm wide and 4.75 cm long. The slits can be interchanged easily and fit into a guide that holds the center of all of the slits at the same place. Each slit is approximately 12.5 mm in height and its center is approximately 9.5 cm above the baseplate.

After the beam of radiant energy enters slit S1, it is reflected from a small diagonal mirror G1 to a spherical collimating mirror G2. The optical path from slit S1 to mirror G2 is equal to approximately 60 cm, the focal length of the mirror. Therefore, the beam of energy directed from mirror G2 to the grating GR, is nearly collimated. Depending on the angular position of the grating, certain wavelengths of energy are diffracted in a near parallel beam to mirror G3, which has the same focal length as mirror G2. The radiant energy incident on mirror G3 is dispersed, with different wavelengths incident on the mirror at different angles. Energy of a single wavelength is focused by mirror G3 onto the grid assembly, forming an image of the entrance slit.

Figure 8 shows the central ray of a beam of monochromatic energy passing through the grid of the grid assembly. Before passing through the grid, the energy beam first strikes mirror G4, which is tilted  $45^\circ$  from the vertical. Mirrors G4 and G5 are normal to each other so that the central ray returns to mirror G3 parallel to, but displaced upward from, the ray before it strikes mirror G4. The grid may contain more than one opening although the one illustrated contains a single opening and passes one narrow spectral interval.

The central ray from the center of the slit to the center of the grating travels in a plane parallel to the baseplate of the instrument until it strikes mirror G4. The ray from mirror G5 to G3 is also parallel to the baseplate, but after striking mirror G3 it is directed slightly downward to the center of the grating. From there it continues downward until it strikes mirror G2 at a point approximately 1.8 cm below the point where it was incident on mirror G2 in the incoming beam. Except for the slight change in the vertical angle, the returning beam strikes the grating in exactly the reverse of the path on which it entered. Thus the grating undisperses the beam of energy passed by the retroreflector-grid assembly so that the image formed at the exit slit S2 is undispersed.

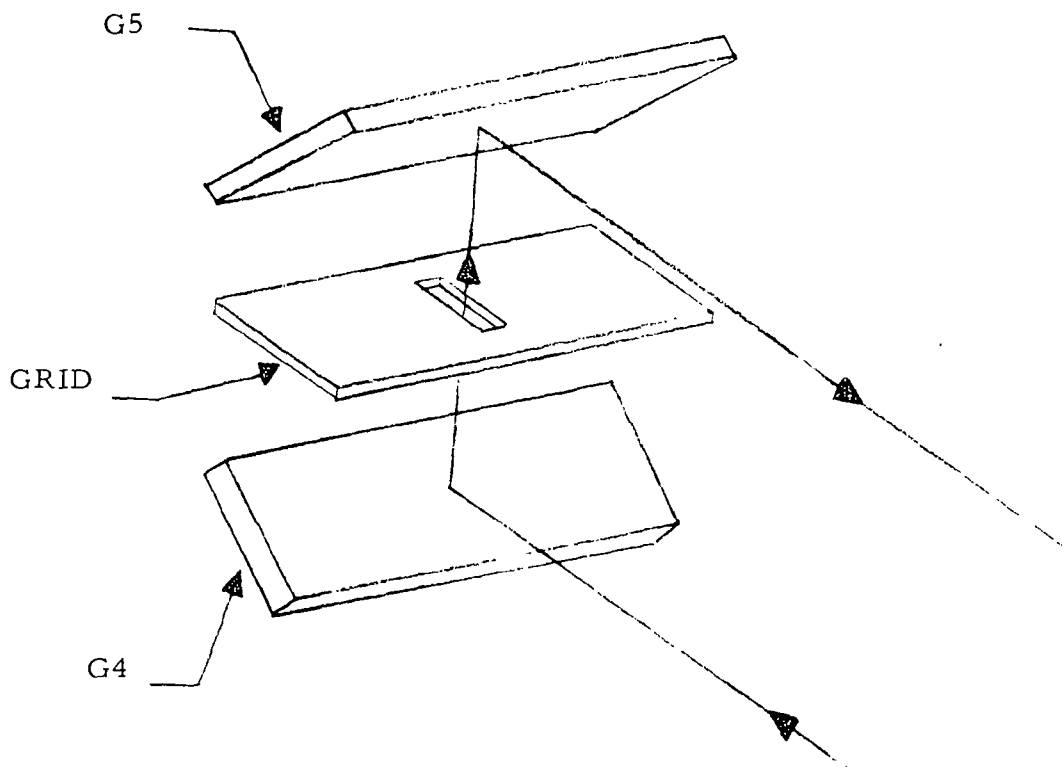


Figure 8. Optical diagram of the retroreflector-grid assembly.

The center of slit S2 is 7.7 cm above the baseplate, approximately 1.8 cm below the center of the entrance slit S1. Because an image of slit S1 is formed at slit S2, only one of these slits is required to provide the desired spectral resolution. Slit S2 is intentionally made somewhat wider than slit S1; the effective part of S2 is only that portion conjugate to the narrower S1. Using the slightly oversize slit S2 instead of a much larger opening reduces scattered energy reaching the detector; having it oversized does not degrade the resolution and makes the positioning of the slits much less critical than if both slits were the same width.

The method by which the radiation is dispersed and the selected portion is recovered and imaged is described in Reference 3. This paper describes the method that uses a prism as a dispersing element; however, the obvious application to a grating and to systems with a "tailored" bandpass are pointed out. Decker<sup>5</sup> has also described an application of the method to Hadamard spectroscopy.

---

5. Decker, J. A. Jr. Experimental Realization of the Multiplex Advantage with a Hadamard-Transform Spectrometer. *Appl. Opt.* 10, No. 3, 510-514, 1971.

## SELECTION OF SPECTRAL BANDPASS

The optical diagram in Figure 9 is useful in deriving and understanding the relationship between the angular position of the grating and the wavelength passed by the grating section. If the entrance slit S1 is very narrow, the horizontal projection of the beam going from mirror G2 to the grating is essentially parallel. The ray AO in Figure 9 can be considered the central ray of this parallel beam; the central ray OB corresponds to the central ray of the monochromatic beam that strikes mirror G3 at such an angle that it is focused on the center of the grid in the retroreflector.

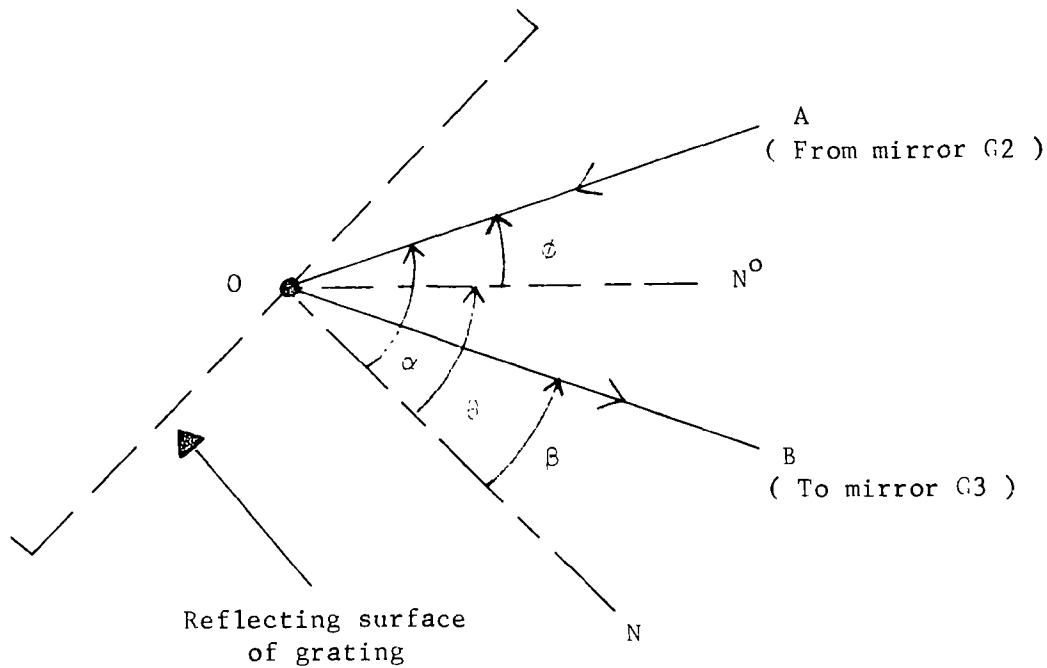


Figure 9. Optical diagram defining angles that relate the grating position to the wavelength of energy passed by the grating assembly. Angles  $\alpha$ ,  $\beta$ , and  $\theta$  are measured from line  $ON$  and are positive in the counter-clockwise direction. Angle  $\phi$  is always positive and is independent of the rotation of the grating.

Consider the situation with the grating rotated about a vertical axis through point O from the typical operating position to the position where its normal ON coincides with the line ON<sup>0</sup>. In this case, both the incoming and reflected rays form the angle  $\phi$  with the normal to the grating. This position of the grating is called the "zero-order" position, and some of the energy of all wavelengths is reflected parallel to OB as if the grating were a plane mirror. In typical operation, the grating is rotated from the zero-order position by an angle  $\theta$  so that its normal is in the position indicated by the line ON in Figure 9. Four angles are defined by the figure and are inter-related by the following equations:

$$\alpha = \theta + \phi. \quad (23)$$

$$\beta = \theta - \phi. \quad (24)$$

$$\alpha + \beta = 2\theta. \quad (25)$$

$$\alpha - \beta = 2\phi. \quad (26)$$

With the grating in the position indicated in Figure 9, the only wavelengths of energy diffracted parallel to the line OB are those for which there is constructive interference. These wavelengths pass through the center of the grid and are given by:

$$m\lambda = 2D \cos \phi \sin \theta, \text{ or} \quad (27)$$

$$m\lambda = D(\sin \alpha + \sin \beta). \quad (28)$$

D is the distance between the adjacent rulings on the grating, and m is an integer. The first order wavelength is the longest one passed and corresponds to  $m = 1$ ; higher orders correspond to  $m = 2, 3, \dots$  etc. Note that the zero-order position of the grating corresponds to  $\theta = 0$  and  $m = 0$ ; in this position,  $\beta$  is negative and  $\sin \alpha = -\sin \beta$ . In the following discussion  $m = 1$  unless otherwise indicated.

The wavelength  $\lambda_c$  of the radiant energy passing through the center of the grid is adjusted with the screw mechanism shown in Figure 1. As the screw rotates, the nut moves along the axis of the screw and drives the arm on the grating assembly, changing angle  $\theta$  while  $\phi$  remains fixed. A linear scale on the side of the screw mechanism makes it easy to measure the displacement of the nut from the end of the screw opposite the screw handle. One complete revolution of the screw produces a displacement of 1 mm, or one grating count. A scale on the outside surface of the drum to which the handle is attached makes it possible to read the grating counts directly to 0.01.

From the calibration curves in Figure 10 it is possible to determine the wavelength passed by the grating from the grating counts without determining the values of any of the angles. The values of wavelength and wavenumber, written in parentheses in the left-hand panel, correspond to the grating with 150 lines/mm.

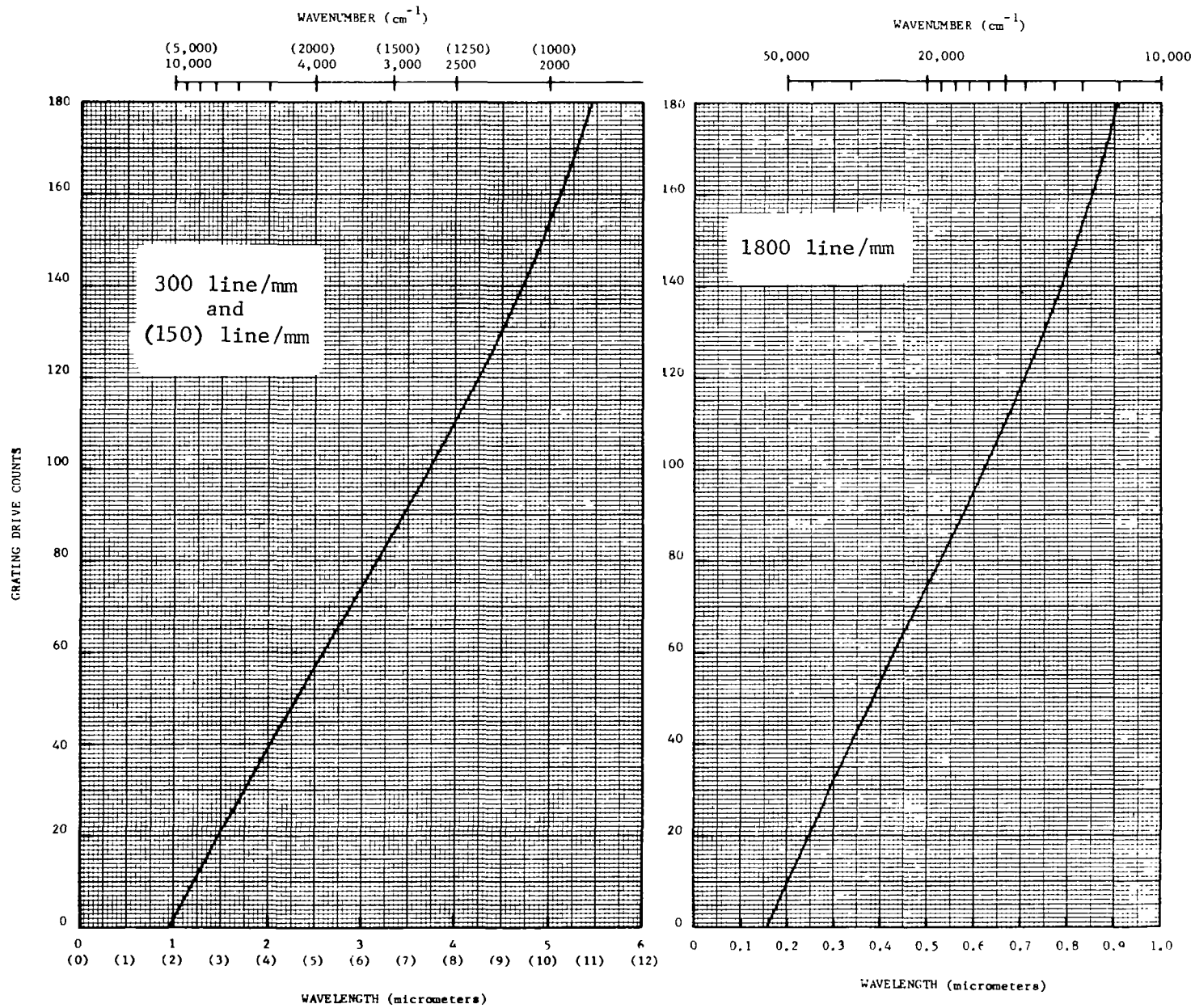


Figure 10. Calibration curves relating the grating drive counts to wavelength and to wavenumber. The numbers in parentheses correspond to the 150 line/mm grating.

The other values, not in parentheses, represent the 300 line/mm grating. The right-hand panel of Figure 10 is the corresponding plot for the 1800 line/mm grating used in the uv, visible, and near infrared. Each grating is blazed at the following wavelength: 150 line/mm at 6  $\mu\text{m}$ , 300 line/mm at 3  $\mu\text{m}$  and 1800 line/mm at 0.50  $\mu\text{m}$ .

It is apparent from Figure 9 and Equation (28) that energy of wavelength  $\lambda_c + \delta\lambda$  will not be diffracted with constructive interference through exactly the same angle  $\beta$  as will energy of wavelength  $\lambda_c$ , which passes from the center of the entrance slit to the center of the grid. The difference  $\delta\beta$  between the angles at which the two nearby wavelengths leave the grating can be determined from Equation (28). Because the central rays for the beams of the two different wavelengths are incident on mirror G3 at different angles, the two wavelengths are focused at different positions in the plane of the grid. The distance  $\delta g$  between the two images of the two different wavelengths in the plane of the grid is given by

$$\delta g = f (\delta\beta), \quad (29)$$

where  $f$  is the focal length of mirrors G2 and G3. The dispersion,  $\delta\lambda/\delta g$ , in the plane of the grid can be calculated from Equations (28) and (29) by holding  $\sin \alpha$  constant and differentiating Equation (28) with respect to  $\beta$ . If we assume a very narrow entrance slit, the result of this dispersion calculation provides the distance between two different wavelengths in the plane of the grid. In many cases it is preferable to express dispersion in wavenumbers per millimeter, rather than in micrometers per millimeter. When  $\nu$  is expressed in  $\text{cm}^{-1}$  and  $\lambda$  in micrometers,

$$\delta\nu = - \frac{\delta\lambda \times 10^4}{\lambda^2}. \quad (30)$$

The solid curves in Figure 11 relate the dispersion in  $\text{cm}^{-1}$  per mm in the plane of the grid to wavenumber and wavelength for first-order radiation. If the physical width  $W_n$  of the entrance slit is much narrower than the width  $W_g$  of an opening in the grid, the spectral interval  $\delta\nu$  passed by the grid is given by

$$\delta\nu (\text{cm}^{-1}) = W_g (\text{mm}) \frac{\delta\nu}{\delta g} (\text{cm}^{-1} \text{ per mm}). \quad (\text{for } W_n \ll W_g) \quad (31)$$

Consider the image of the entrance slit that is formed at the plane of the grid for monochromatic energy with a perfect optical system; i.e., one for which there are no aberrations and the diffraction-limited image size is very small compared to the physical slitwidth. The spread  $\delta\alpha$  in the beam incident on the grating is

$$\delta\alpha = W_g / f. \quad (32)$$

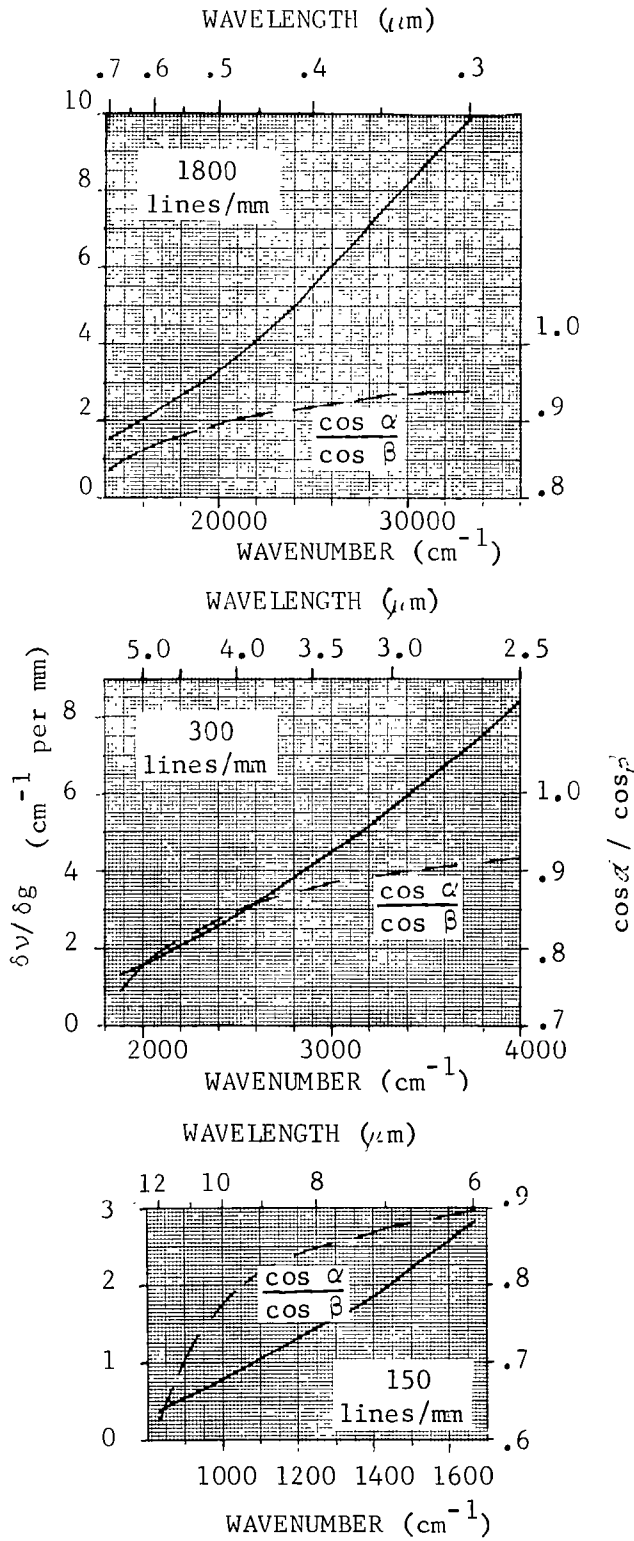


Figure 11. Curves of  $\delta\nu/\delta g$  and  $\cos \alpha/\cos \beta$  vs wavenumber for the three gratings.

By differentiating the quantities in Equation (28) we can show that for constant  $\lambda$

$$\frac{\delta\beta}{\delta\alpha} = - \frac{\cos \alpha}{\cos \beta}. \quad (33)$$

Thus, the width of the image at the grid plane =  $W_n \times \delta\beta/\delta\alpha$ . The negative sign in the equation refers to the relative directions in the changes of the angles.

When  $W_n$  is not negligible in comparison to  $W_g$ , the width of an opening in the grid, the "transmission function" of each opening in the grid is "trapezoidal" and is represented by Figure 12. In most applications of the instrument described in this report,  $W_n \cos \alpha / \cos \beta < W_g$ . The maximum effective  $W_n$  is limited to approximately 1.6 mm, the width of the image of the source on slit S1. Values of  $\cos \alpha / \cos \beta$  can be obtained from the curves of Figure 11.

The aberrations in the optics of the grating assembly produce a blurring of less than 0.1 mm, and the diffraction-limited image width is also less than 0.1 mm, except for  $\lambda$  greater than about 8  $\mu\text{m}$ . Therefore, the simple method of determining the transmission function just described is approximately valid if either  $W_n$  or  $W_g$  is greater than about 0.1 to 0.2 mm. For narrower slits or grid openings, the spectral bandpass is somewhat greater than would be calculated by the simple method that ignores aberrations and diffraction limitations.

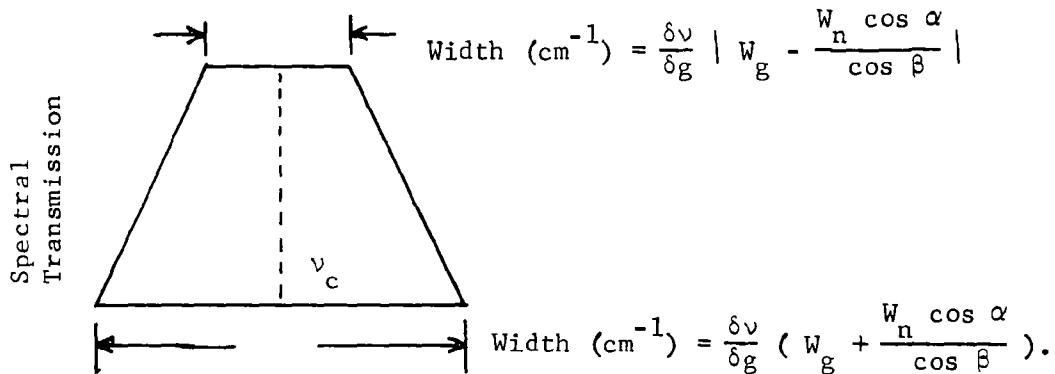


Figure 12. Plot of trapezoidal slit function.

## SECTION IX

### ELECTRONICS AND PROCESSING OF DETECTOR SIGNAL

The electronics process the signal from the photodetector and produce a dc voltage that is proportional to the concentration of the gas species being measured. The relationship between the output voltage and the gas concentration is determined by calibrating the instrument with samples of known concentration. During the normal mode of operation, the spectral interval passed by the instrument remains fixed, and the sample gas is placed in the sample cell. Zero-readings are made by evacuating the sample cell or by filling it with a non-absorbing gas. In addition to the normal mode of operation, the instrument can be used to measure the transmittance of radiant energy by gases or other materials, such as windows. This can be done with the wavelength fixed, or spectral curves of transmittance can be obtained while the wavelength is being scanned continuously.

The electronic components are contained in the compartment indicated in Figure 1. The preamplifiers and amplifiers are mounted on circuit cards and are easily accessible by removing the cover of the electronics compartment. The switches, controls, panel meter, and recorder output jacks are mounted on the removable cover. All of the electronic circuits for the H<sub>2</sub>O monitor described in Section X are also included in the same electronics compartment.

A block diagram of the electronics used to process the photodetector signal is shown in Figure 13. The 360 Hz component of the signal from the photodetector serves as the carrier for the 30 Hz component that is to be measured. The detector signal resulting from any 30 Hz variation of radiant energy on the detector that is not also chopped at the carrier frequency is rejected by the electronics. The electronics consist basically of two synchronous demodulators in series. The first demodulator operates at the carrier frequency, and the average dc component is proportional to the amount of radiant energy chopped at 360 Hz. If the chopped energy incident on the detector is also modulated at 30 Hz, the 30 Hz component of the signal output of the 360 Hz synchronous demodulator is proportional to the modulation. This 30 Hz component then passes through a series of gain controls and amplifiers to the second synchronous demodulator that operates at 30 Hz. The output of the second synchronous demodulator is then proportional to the 30 Hz modulation, and thus to the concentration of the gas species being measured.

When H<sub>2</sub>O in the sample interferes with the gas species being measured, the 30 Hz signal also contains a component due to the H<sub>2</sub>O. This interference is accounted for by an H<sub>2</sub>O monitor described in Section X that produces a dc signal proportional to the H<sub>2</sub>O concentration. An adjustable portion of the

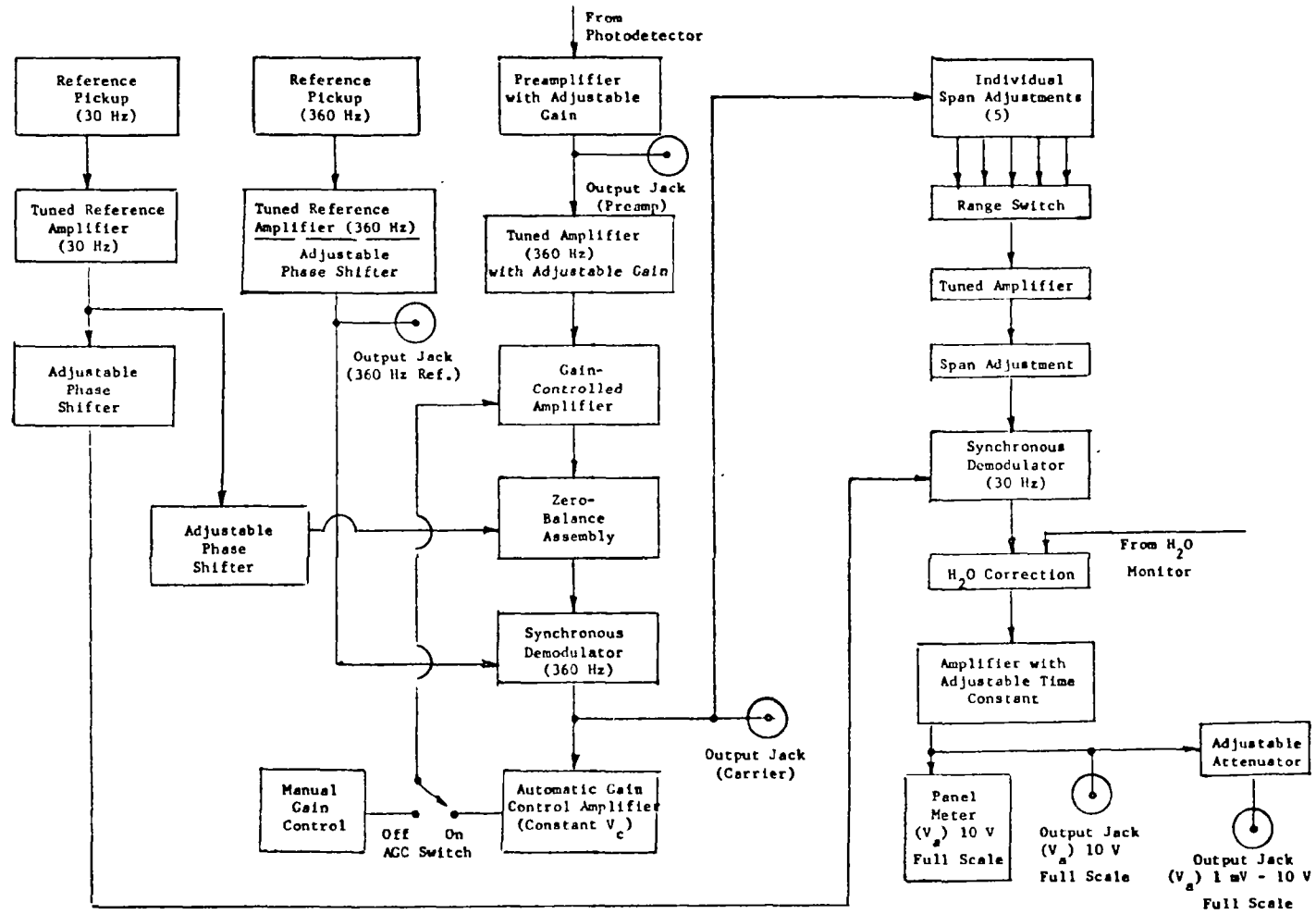


Figure 13. Block diagram of electronics.

output of this H<sub>2</sub>O monitor is fed into the "H<sub>2</sub>O Correction" circuits in the place indicated in the block diagram of Figure 13. The signal output from the H<sub>2</sub>O correction circuits has been automatically corrected for any interference by H<sub>2</sub>O in the sample and is proportional to the concentration of the gas species being measured. The electronic components used to adjust the portion of the H<sub>2</sub>O monitor output that is fed into the correction circuits are discussed as part of the H<sub>2</sub>O monitor in Section X.

A five position switch makes it possible to select an electronic time constant of 0.3, 1, 3 or 10 sec. When the switch is in the fifth position, marked "off", no additional damping is applied to the signal and the effective time constant is approximately 0.1 seconds. The main signal output can be determined from a panel meter or from either of two output jacks. A signal that corresponds to a full-scale reading of the panel meter produces a 10 volt dc signal on one of the output jacks. The corresponding full scale reading for the other output jack can be adjusted from less than 1 mv to 10 v. Thus, the instrument can be used with a wide range of recorders or meters, provided the input impedance is sufficiently high.

As discussed in Section V, it is desirable that the signal output during the normal mode of operation be proportional to the ratio,  $V_a/V_c = V'$ . The instrument calibration relates the concentration of the gas being measured to  $V'$ , and it is desired that this relationship be independent of source brightness, detector sensitivity, etc. During the normal mode of operation  $V_c$  is maintained at a constant value by the AGC circuits. If, for example, the signal from the photodetector decreases because of dirt on a window or a decrease in source brightness, the gain of the gain-controlled amplifier increases to maintain  $V_c$  constant. The increase in gain also increases the amplification of both the 360 Hz signal and the 30 Hz signal by the same factor. Therefore,  $V'$  is kept directly proportional to the output  $V_a$  and maintains a constant relationship with the gas concentration. The AGC circuits can account for changes in the 360 Hz component of the signal from the preamplifier by approximately a factor of 4. When the AGC switch is in the off position,  $V_c$  is not maintained constant but can be adjusted with a manual gain control.

Both reference pickups consist of a light-emitting diode (LED) and a small phototransistor. The 360 Hz pickup is mounted near the high-speed chopper so that the output is modulated as the spokes of the chopper pass between the LED and the phototransistor. The 30 Hz pickup senses the light from the LED that is reflected by the mirror chopper. The amplifier for each reference pickup is tuned and contains an adjustable phase shifter to produce a "clean" signal with the proper phase for the synchronous demodulators.

The zero-balance assembly electronically accounts for any misbalance between the two beams passing through the two legs of the alternator when there is no absorbing gas in the sample cell. This electronic assembly would not be required if it were practical to maintain a perfect optical balance between the two legs. Approximately  $\pm 10$  percent variation in the transmittance through either of the legs of the alternator can be accounted for by this electronic zero-balance assembly. The assembly changes the amplification ahead of the 360 Hz synchronous demodulator during the two halves of the alternator cycle. A signal from the 30 Hz reference pickup switches the zero-balance assembly between the two different gains with the proper phase. The difference in the

gains between the two halves is adjustable by the "zero" potentiometer on the top of the electronics compartment.

Five ranges of sensitivity are provided. The gain in each range can be adjusted independently over a factor of approximately 5. A five-position switch mounted on the top of the electronics compartment makes it convenient to change from one range to another. An additional potentiometer is also provided to change the gain of all 5 ranges simultaneously by the same factor. At the time the instrument was delivered to EPA, the range adjustments, also called span adjustments, were made so that full-scale output corresponded to  $V' = 0.003, 0.01, 0.03, 0.1$  and  $0.30$ .

Three additional output jacks are provided on the cover of the electronics compartment. One output jack, labeled "preamp", makes it possible to monitor the electronic signal from the preamplifier before it passes through the tuned filters or amplifiers. The output of the 360 Hz demodulator can also be monitored from the output jack labeled "carrier". The transmission of gas samples, attenuators, windows, or other optical components can be measured easily by monitoring the output from this recorder jack while the AGC switch is in the off position. Spectral curves of transmittance of gases can be obtained by recording the signal from this jack while the grating is being scanned. The 360 Hz reference signal is also available from another output jack. Having this signal readily accessible is convenient if a separate synchronous demodulator is used to scan spectra or make other transmission measurements.

A four-position switch mounted near the panel meter makes it possible to use the same meter to monitor other quantities besides the signal output. The 30 Hz reference signal and the average carrier voltage  $V_c$  can be checked with this meter to see if they are in the right operating range. When the instrument is operating in the normal mode with the AGC switch turned on, the carrier signal produces approximately 50 percent of full-scale reading of the panel meter. While the selector switch is in the "signal-in" position, the meter reads the level of the signal going into the 360 Hz synchronous demodulator.

## SECTION X

### H<sub>2</sub>O MONITOR

#### OPTICAL

The H<sub>2</sub>O monitor produces a dc voltage that is proportional to the concentration of H<sub>2</sub>O in the multiple-pass sample cell. The output voltage is displayed on a panel meter and can be fed into the main electronic circuit to automatically account for any interference by H<sub>2</sub>O in the sample. The H<sub>2</sub>O concentration is determined by comparing the transmission of the sample at two wavelengths, one in the region of strong H<sub>2</sub>O absorption near 1.9  $\mu\text{m}$  and one in a nearby region of weak absorption.

Two views of the optical layout of the H<sub>2</sub>O monitor are shown in Figure 14. A small tungsten iodide bulb serves as a source of infrared radiant energy. The beam is interrupted at 360 Hz by a small, 6-bladed chopper that is rotated at 3600 rpm by a synchronous motor. The position of the transmitting optics on the multiple-pass sample cell is shown in the left-hand portion of Figure 14 and in the photograph in Figure 5.

After the beam enters the multiple-pass sample cell through window W3, it is reflected by a small flat mirror H1 to spherical mirror C2, which is shown in Figure 1 but not in Figure 14. Mirror C2 directs the beam back to another flat mirror H2 and down through the exit window W4, which is mounted on the underneath side of the sample cell. An image of the source is formed near the small flat mirror H3, which is tilted 45° from the vertical and directs the beam to the receiving optics that include the detectors and filters. Window W3 is a small plano-convex lens that enlarges the image of the source near mirror H3. Windows W3 and W4 are bonded to the stainless steel body of the sample cell with silicone rubber cement. Mirrors H1 and H2 are each bonded with epoxy cement to a small aluminum block that is bolted to the cell wall.

Detectors A and B have photoconductive PbS elements, 4 mm x 4 mm, that are mounted on a small aluminum block as shown in Figure 15. Lens L4 forms images of mirror C2 on the detectors. Filter A acts as a dichroic beam-splitter, transmitting a narrow spectral interval in the region of strong H<sub>2</sub>O absorption near 1.9  $\mu\text{m}$ . The wavelengths not transmitted by filter A are reflected to filter B, which transmits a narrow spectral interval of weak H<sub>2</sub>O absorption. The gains of the preamplifiers are adjusted so that the 360 Hz signals from the two detectors are equal when no absorbing gas is in the sample cell. It is apparent that the addition of H<sub>2</sub>O to the sample cell would reduce the amount of energy incident on detector A more than that on detector B. The resulting difference in the detector signals is proportional to the H<sub>2</sub>O concentration.

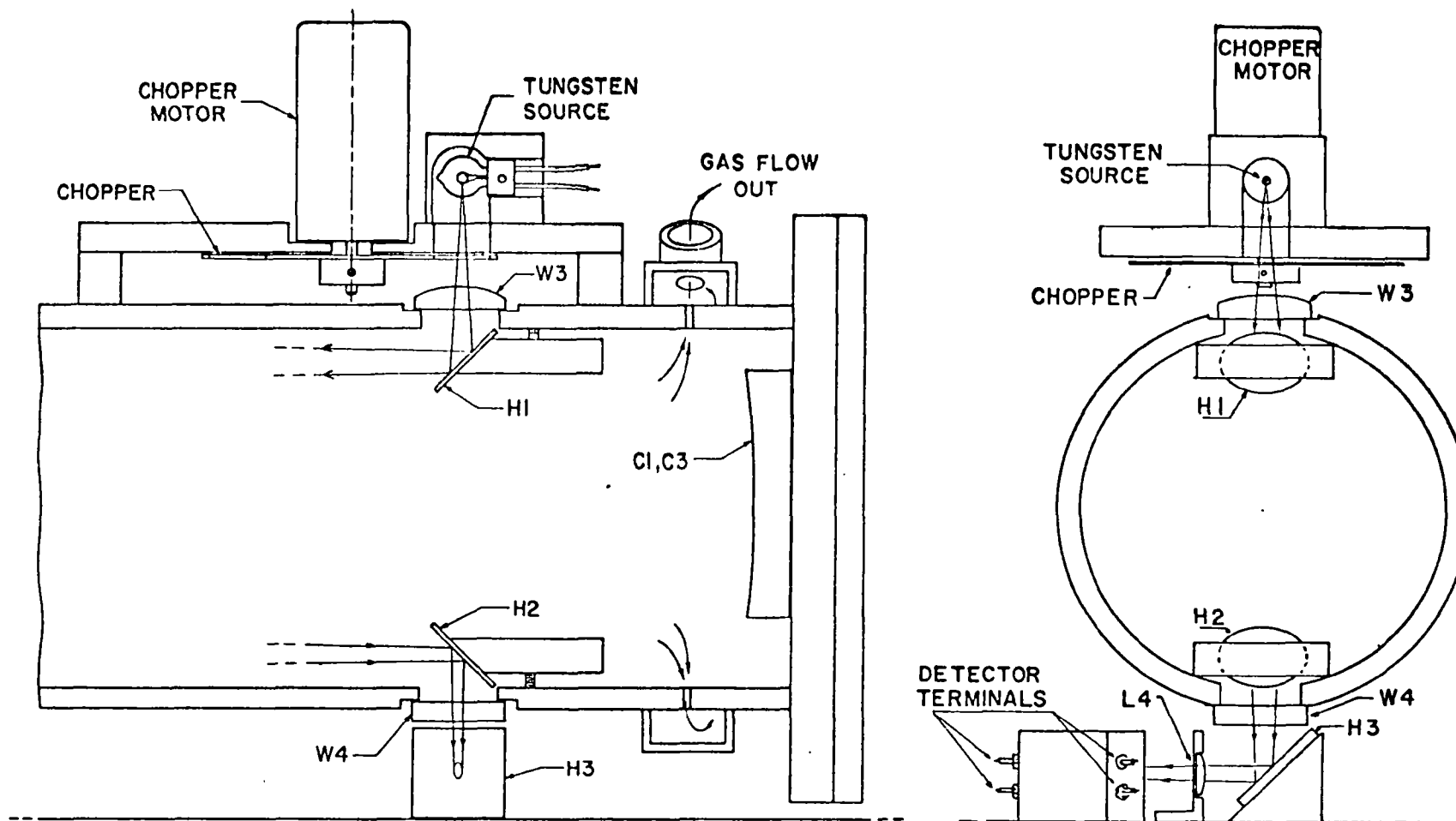


Figure 14. Two optical diagrams of the  $H_2O$  monitor.

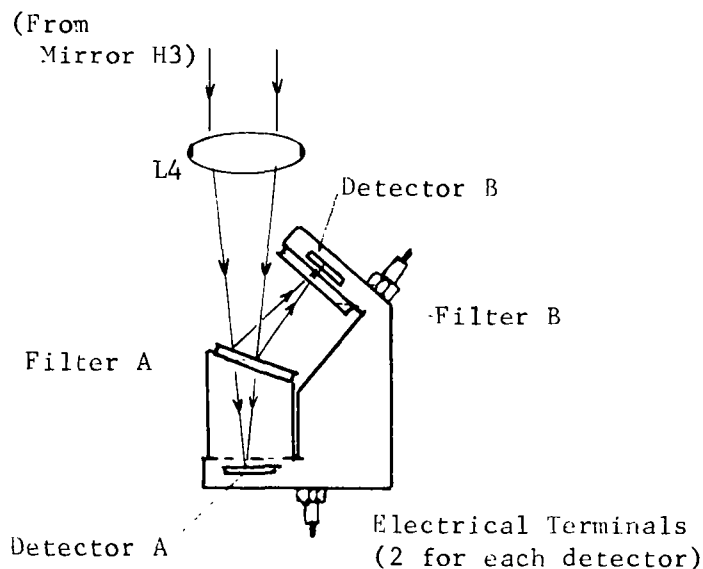


Figure 15. Diagram of the receiving optics for the H<sub>2</sub>O Monitor.

Small variations in the temperatures of the detectors can produce drift in the zero-reading of the monitor, making it less stable than monitors that employ only one detector. However, we have found from experience with similar instruments that this 2-detector type of monitor is quite adequate for the present purposes. Ordinarily the correction for H<sub>2</sub>O interference in the main instrument channel is small so that the size of the correction signal from the H<sub>2</sub>O monitor need not be highly accurate. By employing two fixed filters and two detectors, it is possible to keep the optics relatively simple without any moving optical components other than the simple chopper.

#### SIGNAL PROCESSING

The bias voltage for detectors A and B is provided by a  $\pm 15$  v dc supply used with the main electronics. A separate preamplifier amplifies the output of each detector, and the outputs of both preamplifiers are fed into a difference amplifier. When the sample cell is free of any H<sub>2</sub>O, the monitor is zeroed by adjusting the outputs of the preamplifiers so that they are equal, producing a zero input to the difference amplifier. The addition of H<sub>2</sub>O to the sample cell creates a misbalance between the signals from the two preamplifiers and results in a signal from the difference amplifier. This signal passes through a tuned amplifier and is then demodulated to produce a dc voltage that is proportional to the H<sub>2</sub>O concentration. A reference signal for the synchronous demodulator is obtained from the output of the preamplifier for detector B.

A variable-gain amplifier makes it possible to adjust the "span" so that full-scale readings of the panel meter can be made to correspond to H<sub>2</sub>O concentrations between approximately 1 percent and 10 percent. An output jack connected in parallel with the panel meter has an adjustable attenuator that can be used

to vary the signal at the output jack that corresponds to full-scale reading of the meter from less than 1 mv to 10 v dc.

An adjustable fraction of the output of the variable-gain amplifier is fed into the main electronics as indicated in Figure 13 to correct the signal output for interference by H<sub>2</sub>O in the sample. The "correction factor" is adjusted to control the correction signal so that it is of the proper size and polarity. Interference by H<sub>2</sub>O is positive for some gases and negative for others; thus it is necessary that the polarity of the correction signal be changeable. In order to adjust the correction factor, N<sub>2</sub> or argon is bubbled through water and through the sample cell to produce an H<sub>2</sub>O concentration approximately equal to that expected in the samples to be studied. The potentiometer used to change the correction factor is then adjusted to cancel any signal from the main electronics that results from interference by the H<sub>2</sub>O. With the H<sub>2</sub>O correction adjusted in this manner, the proper correction signal is applied for all H<sub>2</sub>O concentrations over a wide range that includes the concentration used in making the adjustments.

If the H<sub>2</sub>O concentration is less than approximately 2 percent, the relationship between the concentration and the output of the H<sub>2</sub>O monitor is nearly linear. A similar linear relationship also exists between the output of the main electronics and the concentration of the gas species being measured when the concentration is low. When the concentrations of H<sub>2</sub>O and the gas being measured are both in the linear region, the correction factor is valid for all concentrations when it is adjusted as described above. However, because of the slight non-linearity in the responses, a single adjustment of the correction factor made at one H<sub>2</sub>O concentration may not be valid for concentrations that are quite different. Therefore, it is best to follow the above adjustment procedure and use H<sub>2</sub>O concentrations similar to those expected in the samples. When measuring formaldehyde concentrations, the interference by H<sub>2</sub>O is relatively small so that it can be corrected adequately for all H<sub>2</sub>O concentrations up to 4 percent with a single setting of the correction factor. A different setting may be required if higher H<sub>2</sub>O concentrations occur in the samples.

An automatic gain control circuit is employed so that the amplified difference signal is nearly independent of slight changes in such things as source brightness or dirt on windows that would change the amount of energy incident on both detectors by about the same factor. The AGC maintains the signal from the pre-amplifier for detector B at a constant level. For example, if a change in the optics occurs that would ordinarily decrease the detector signal, the bias voltage is increased automatically to compensate for the decrease in radiant energy. The bias voltages for both detectors are increased by the same factor; therefore, to a good approximation, the change in bias voltage increases the outputs of both detectors by the same factor. It follows that a given output of the difference amplifier represents a certain fractional difference in the outputs of the two preamplifiers. This difference can then be related to the H<sub>2</sub>O concentration and is nearly independent of small changes in source brightness, dirt on windows, etc.

## SECTION XI

### RESULTS OF FORMALDEHYDE TESTS

#### SPECTRAL BANDPASS SELECTION

By investigating a high-resolution spectrum of formaldehyde provided for us by Dr. Philip Hanst of EPA, we concluded that enough strong spectral structure existed in the 2700 - 3000  $\text{cm}^{-1}$  region for the efficient operation of a gas-filter correlation spectrometer for this gas. It was possible to select several narrow spectral intervals within the 2700 - 3000  $\text{cm}^{-1}$  region that might provide better performance than the full 300  $\text{cm}^{-1}$  wide interval. We decided to assemble the components and use the instrument to determine the optimum of the several promising spectral intervals for use in the normal GFC mode. The two most important factors in the choice of the spectral interval are sensitivity and discrimination against other gases that occur in automotive exhaust.

Among the possible interfering gases are hydrocarbons and  $\text{H}_2\text{O}$ . Although  $\text{H}_2\text{O}$  absorption is relatively weak in this spectral region, a small amount of interference by this gas is almost certain because of its high concentration (typically 2%-3%) and the long sample path lengths required to produce adequate sensitivity to formaldehyde. Interference by  $\text{H}_2\text{O}$  was not considered in the final selection of the bandpass because it was assumed that the  $\text{H}_2\text{O}$  monitor with its correction circuitry could account for the small amount of interference.

Figure 16 shows spectral curves of transmittance for formaldehyde and for five other hydrocarbons that absorb in the same spectral region and may be expected to interfere. All of the curves were scanned with the GFC spectrometer without the gas-filter cell (GFC) in place. The grating counts scale at the top of the figure refers to the position of the grating screw as discussed in Section VIII. The formaldehyde sample was contained in the heated GFC discussed in Section VI. All of the hydrocarbon samples represented in the lower two panels were pure and at 1 atm pressure in a 1 cm sample cell. Acetylene, another hydrocarbon found in automotive exhaust, is not represented in Figure 16 because it does not absorb in this spectral region. The 0.8  $\text{cm}^{-1}$  spectral slitwidth used in scanning the spectra is too wide to show all of the structure in the spectra of formaldehyde, methane, ethylene, and ethane. Little additional structure would be observed in the spectra of propane and butane if narrower slits were employed because the lines are so closely spaced that they blend together when the sample pressure is greater than a few-tenths of an atm.

The hydrocarbon samples represented in Figure 16 contain much more absorbing gas than would be expected in a typical sample of automotive exhaust gas, but the curves point out clearly that excessive interference might be expected if

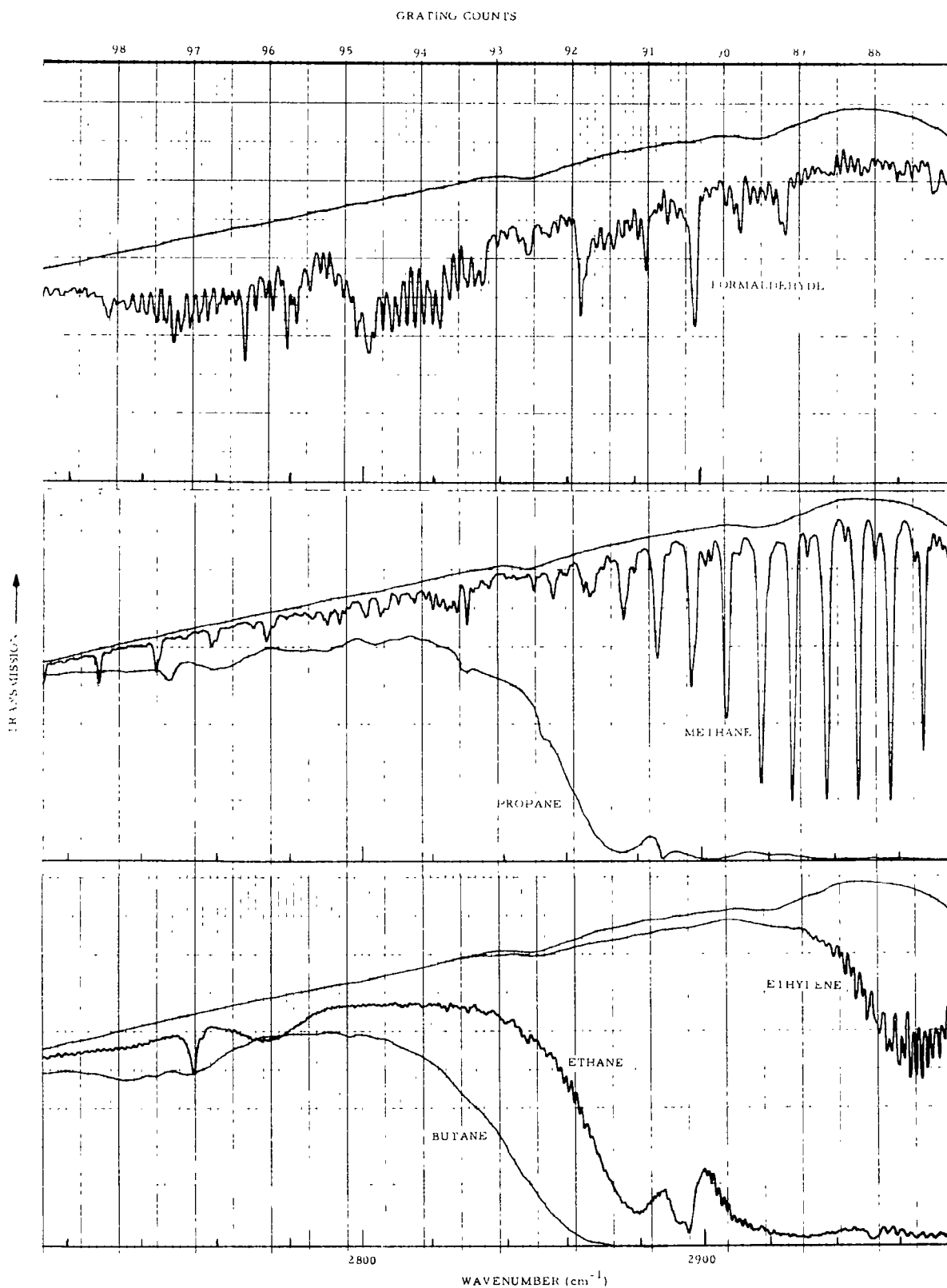


Figure 16. Spectral curves of transmittance for formaldehyde and five hydrocarbons. The smooth, upper curve in each panel corresponds to 100% transmittance and was scanned with the sample cell evacuated. The spectral slitwidth is approximately  $0.8 \text{ cm}^{-1}$ .

the bandpass extended above approximately  $2830\text{ cm}^{-1}$ . Interference tests were made with the GFC instrument operating in its normal mode with several different spectral bandpasses. As expected, troublesome interference by some of the hydrocarbons was observed when the bandpass extended to the higher wavenumbers. Methane is usually present in automotive exhaust at a higher concentration than any of the other hydrocarbons investigated. Thus it is important that interference by this gas be kept as low as is practical. It is likely that the concentration of methane in the samples will also be measured with a separate instrument; therefore, it will be possible to account for a small amount of interference by this gas from a predetermined value of the discrimination ratio.

By conducting several tests for different spectral intervals by the methods described below, we concluded that the optimum spectral bandpass is centered at approximately  $2803\text{ cm}^{-1}$ . A trapezoidal slit function such as the one illustrated in Figure 12 determines the spectral bandpass. The approximate widths of the "top" and the "bottom" of the trapezoid are  $11.4\text{ cm}^{-1}$  and  $18.6\text{ cm}^{-1}$ , respectively. This relatively narrow interval includes enough radiant energy that detector noise is not the major source of error, as would be the case if a much narrower interval were employed. Wider spectral intervals produce more interference by the five hydrocarbons represented in Figure 16. Most of the wider intervals investigated also produced a lower Pembroke factor,  $F$ , than did the selected interval. As discussed in Section V, the lower Pembroke factor would increase the uncertainty caused by turbulence, slight optical misalignment, and other types of optical noise.

#### TEST PROCEDURES AND PERFORMANCE

Formaldehyde samples used in the tests were contained in a small, heated cell that was constructed similar to the GFC. The by-pass optics were put in place as illustrated in Figure 6 so that the beam did not pass through the multiple-pass sample cell. The heated formaldehyde sample cell was placed in the beam adjacent to the by-pass optics. A 1 cm long sample cell replaced the heated sample cell while investigating the interference by other hydrocarbons. In order to use longer sample paths for the study of interference by  $\text{H}_2\text{O}$  and  $\text{CO}_2$ , the by-pass optics were removed and the multiple-pass sample cell was used at 40 passes.

No pressure transducer was included with the sample cell; therefore it was not possible to measure directly the pressure of the formaldehyde vapor in the sample. As in the GFC, a small amount of paraformaldehyde powder was placed in the sample cell, and the vapor was formed as the heated (approximately  $55^\circ\text{C}$ ) powder evaporated. The cell was evacuated to less than 0.001 atm for a minute or less in order to obtain "zero-readings". As soon as the valve on the sample cell was closed, the pressure started increasing again as the powder evaporated. Typically, one-half to one hour was required for the pressure to increase to the desired value for another set of readings. The pressure was not in equilibrium after this relatively short time, but it was nearly constant while a set of measurements was being made. On several occasions, as many as 5 measurements of  $V'$  and either  $\bar{A}_{g+at,s}$  or  $\bar{A}_{at,s}$  were made at intermediate pressures as the pressure was building up, or as the cell was partially evacuated in steps.

As explained below, many of the tests involved measuring the quantities required to determine the correlation efficiency  $C_c$ , and it was not necessary to know the pressure of the formaldehyde vapor except for a few samples. In order to estimate the formaldehyde pressure for a few samples, the values of  $\bar{A}_{at,s}$  were

related to the formaldehyde pressure by using absorption data obtained over the same spectral interval for gas in the GFC at several different pressures. The pressure transducer made it possible to measure the pressure of the vapor in the GFC when its absorptance was measured. After the pressure had been determined in this manner, the absorber thickness was computed and the important Pembroke Factor  $F$  was calculated by use of Equation 20.

Several samples were investigated with  $N_2$  added to the formaldehyde vapor to produce pressures up to 1 atm, the pressure at which most samples of interest will probably be investigated. The  $N_2$  was added to the cell just after it had been evacuated by first pressurizing the line to the cell then opening the cell valve to allow the  $N_2$  to enter. The pressure was measured before the formaldehyde vapor had time to diffuse through the valve and the  $N_2$  to the unheated gas line where it would have condensed. Nitrogen was also added to the vapor in the heated GFC in the same manner in order to investigate the influence of pressure-broadening of the absorption lines.

Because of the difficulties in accurately measuring the pressure of formaldehyde vapor in mixtures containing  $N_2$ , it was decided that we would provide only approximate calibration data to relate  $V'$  to formaldehyde absorber thickness. The Environmental Protection Agency has developed more accurate methods of determining formaldehyde partial pressures; therefore, the final, more accurate, calibration will be performed by EPA scientists after they receive the instrument. The data obtained by us have been limited primarily to small samples for which a nearly linear relationship exists between  $V'$  and the absorber thickness.

During most of the tests the instrument was operated in the normal mode so that  $V'$  could be measured directly. In addition the signal from the output jack labeled "preamp" (see Figure 13) served as the input to a separate amplifier and synchronous demodulator. This demodulator received its reference signal from the output jack labeled "360 Hz Ref.". The demodulator output was proportional to  $V_c$ , the average value of the carrier voltage. By monitoring the output of this demodulator with a strip-chart recorder, we measured the absorptance (or transmittance) of samples as they were introduced into the sample cell or pumped from it.

In accordance with the discussion and definitions in Section V, the absorptance measured for a given sample depends upon the manner by which it is measured. The absorptance  $\bar{A}_{g+at,s}$  is given directly from  $(D_0 - D_s)/D_0$  if the instrument is operating in its normal mode with the alternator switching the beam between the formaldehyde GFC and the attenuator (see Equation (16)). The recorder deflections observed with the sample cell filled and with the sample cell evacuated are  $D_s$  and  $D_0$ , respectively. In order to measure  $\bar{A}_{at,s}$ , the beam through the GFC was temporarily blocked so that the only energy reaching the detector was that passing through the attenuator. The recorder deflections were observed with and without the sample in the cell, just as in the measurement of  $\bar{A}_{g+at,s}$ .

Of course,  $V'$  could not be measured directly with the main electronics while the beam through the GFC was blocked during the measurement of  $\bar{A}_{at,s}$ . Therefore, the following procedure was followed in order to measure both  $V'$  and  $\bar{A}_{at,s}$  for a given sample: After the sample had been in place long enough to be reasonably well stabilized, the value of  $V'$  was observed. The main

electronics were then turned off, the beam through the GFC was blocked, and the deflection  $D_s$  of the recorder connected to the synchronous demodulator was noted. The sample cell was then evacuated and  $D_0$  was noted. Finally, the main electronics were turned back on to observe the zero-reading of  $V'$ . The difference between the two values observed for  $V'$ , with and without the sample, represents the true value of  $V'$ .

From Equations (15) and (17) we see that the correlation efficiency  $C_e$  can be determined from a measurement of  $V'$  and of either  $\bar{A}_{at,s}$  or  $\bar{A}_{g+at,s}$ . It is apparent from the previous paragraph that  $\bar{A}_{g+at,s}$  is much simpler to measure than  $\bar{A}_{at,s}$  while measuring  $V'$ . However, when  $C_e$  is high, between approximately 0.5 and the maximum value of 1.0, the quantity  $\bar{A}_{at,s}$  is considerably greater than  $\bar{A}_{g+at,s}$  and can therefore be measured more accurately. The improved accuracy is particularly important for samples with absorptances of only a few percent. Therefore  $\bar{A}_{at,s}$ , rather than  $\bar{A}_{g+at,s}$  was measured for most of the samples. In a few cases, both  $\bar{A}_{at,s}$  and  $\bar{A}_{g+at,s}$  were measured along with  $V'$ . The results were consistent with Equations (15) and (17) within the estimated uncertainties.

Measuring the quantities required to determine  $C_e$  was much easier than measuring the Pembroke Factor  $F$  because of the above-mentioned difficulties in determining the absorber thickness  $u$ . For a given spectral bandpass and a given set of conditions of the formaldehyde GFC, values of  $C_e$  were quite reproducible and nearly independent of the amount of formaldehyde in the sample provided  $\bar{A}_{at,s}$  was less than approximately 0.2 and the sample pressure remained constant.

Table 1 summarizes the results of the measurements of correlation efficiency  $C_e$  for the recommended spectral bandpass, which is centered at  $2803 \text{ cm}^{-1}$  and has a half-power bandwidth of  $15 \text{ cm}^{-1}$ . The data in the table represent the averages of several sets of measurements. Each group of data, A, B, and C, corresponds to a given condition for the formaldehyde gas-filter cell (GFC). Pure formaldehyde vapor was contained in the GFC for groups A and B. Nitrogen was added to the GFC in order to obtain the data in group C.

For each set of GFC conditions,  $C_e$  is greater at low sample pressures than at the highest pressure (1 atm) investigated. This dependence on sample pressure results from the smoothing of the line structure due to collision broadening of the lines as the pressure increases. It will usually be preferable to operate with sample pressures near 1 atm so the sample can be flushed through the sample cell without using a vacuum pump or a complex system of pressure regulators. The maximum value of  $C_e$  tabulated for 1 atm samples is 0.28, which was observed with enough pure formaldehyde in the GFC to reduce its average transmittance  $\bar{T}_g$  to approximately 0.37. Other data not included in the table indicated that somewhat higher values of  $C_e$  could be achieved by employing even lower transmittances of the GFC. However, the advantage of the small increase in  $C_e$  is probably more than offset by the accompanying decrease in chopped radiant energy that reaches the detector. For optimum performance, it is recommended that the GFC be operated with the temperature, and thus the formaldehyde vapor pressure, adjusted to produce an average transmittance  $\bar{T}_g$  between 0.3 and 0.4.

The data in group C of Table 1 were obtained in order to see if  $C_e$  might be improved by adding  $N_2$ , or any non-absorbing gas, to the GFC to broaden the absorption lines. It is most meaningful to compare data group B with group C

TABLE 1

SUMMARY OF MEASUREMENTS OF  
CORRELATION EFFICIENCY  
FOR FORMALDEHYDE

Group	<u>GFC Parameters</u>				Correlation Efficiency $C_e$
	Formaldehyde Pressure (atm)	Total Pressure (atm)	Average Transmittance $\bar{T}_g$	Sample Pressure (atm)	
A	0.070	0.070	0.37	1.00	0.28
				0.50	0.39
				0.20	0.50
				0.10	0.53
B	0.051	0.051	0.48	1.00	0.19
				0.50	0.26
				0.20	0.40
				0.10	0.50
C	0.044	0.50	0.51	1.00	0.16
				0.50	0.24
				0.10	0.28

because  $\bar{T}_g$  is approximately the same for both groups. It is apparent that  $C_e$  is not improved by broadening the lines of the gas in the GFC so they more nearly match the widths of the lines of the sample gas. In fact,  $C_e$  is decreased slightly by the increased GFC pressure, even when the sample pressure is the same as the GFC pressure, or higher. As might be expected,  $C_e$  is lower for high GFC pressures than for low GFC pressures when the sample pressure is 0.1 atm. At this low sample pressure, full advantage of the sharp structure in the spectra is not realized if the spectral structure of the lines of the gas in the GFC is not also sharp.

The average transmittance,  $\bar{T}_g$ , of the vapor in the GFC was measured at several pressures up to approximately 0.1 atm. The spectral bandpass was the same as that used for the data represented in Table 1. The results indicate that the average absorption coefficient  $\bar{k}_s$  for this spectral interval is approximately  $4.0 \text{ (atm cm)}^{-1}$ . From Equation (22), we see that the Pembroke Factor  $F$  can be determined from the values of  $C_e$  listed in Table 1.

$$F \text{ (atm cm)}^{-1} = \frac{C_e \times 4 \text{ (atm cm)}^{-1}}{2} = 2C_e \quad (34)$$

It follows from Equations (18) and (19) that  $V'$ , the quantity measured by the instrument, can be related to  $C_e$ . For samples of low concentration  $c$  (ppm)

at 1 atm pressure in the 40-meter cell when the GFC parameters are the same as those indicated in group A of Table 1,

$$\begin{aligned}
 V' &= F_u = 2 \text{ (atm cm)}^{-1} C_e \times c \text{ (ppm)} \times 4 \times 10^3 \text{ cm} \times \\
 &10^{-6} \text{ (atm x ppm}^{-1}\text{)} = 2.24 \times 10^{-3} c.
 \end{aligned}
 \tag{35}$$

Discrimination against hydrocarbons is quite good when using the spectral bandpass centered near  $2803 \text{ cm}^{-1}$  that was recommended above. As might be expected from the curves in Figure 16, there is no measurable interference by ethylene because the absorption by this gas is negligible in the spectral region of interest. Although both butane and propane absorb significantly in this region, there is little structure in the spectral curves. Consequently, the gas-filter method discriminates quite effectively so that large discrimination ratios are observed: +1000 for propane and -2000 for butane. The interference by ethane is so slight that it could not be measured reliably; the discrimination ratio is probably  $> 5,000$ .

The discrimination ratio for methane is also quite high and is sensitive to changes in the bandpass. By adjusting the center of the bandpass to several positions within a  $4 \text{ cm}^{-1}$  interval, the discrimination ratio was made to vary from approximately +66 to  $\infty$  (no measurable interference) to -500. Thus, if the methane concentration is high enough that very good discrimination is required, a slight "tuning" of the bandpass may be made by placing a methane sample in the cell and nulling the interference. Changes of only 1 or  $2 \text{ cm}^{-1}$  in the center of the bandpass has only a very slight influence on the sensitivity to formaldehyde.

When the  $\text{H}_2\text{O}$  correction circuitry was de-activated, a sample of 2 percent  $\text{H}_2\text{O}$  in  $\text{N}_2$  at 1 atm total pressure produced an output that corresponds to approximately 0.25 ppm of formaldehyde. This corresponds to a discrimination ratio of 80,000 for  $\text{H}_2\text{O}$  without using the  $\text{H}_2\text{O}$  monitor and the correction circuits. When the  $\text{H}_2\text{O}$  correction circuits are employed and adjusted properly, the apparent remaining error due to a 5 percent  $\text{H}_2\text{O}$  mixture is less than 0.05 ppm of formaldehyde.

When the interference by other gases is negligible, the minimum detectable concentration is limited by the noise on the output signal of the instrument when it is operating in the normal mode. Most of this noise comes from two basic sources, detector noise and "optical" noise. The relative contribution by each source depends on the operating condition. The amount of noise produced by the PbS detector is essentially independent of the amount of chopped energy incident upon it. Therefore, the relative amount of detector noise can be observed by blocking the beam of chopped energy from the detector. Of course, the automatic gain control must be turned off during this measurement so that the amplifier gain remains constant when the chopped energy is blocked. Noise generated by the pre-amplifier and the other electronics that process the detector signal is much less than the noise generated by the detector. For the sake of the present discussion, this small amount of amplifier noise can be treated as part of the detector noise

because its magnitude is essentially independent of the amount of chopped energy incident on the detector.

In the present discussion, optical noise is defined as the noise in the output signal that results from variations in the amount of chopped energy incident on the detector. Thus, if the minimum detectable concentration is limited by optical noise, the signal-to-noise ratio cannot be improved by merely increasing the chopped energy. Optical noise may be caused by turbulence and other types of beam steering due to non-uniformities in the temperature or composition of the gas in the optical path. Instabilities in mirrors, lenses, choppers, and other optical components may also contribute to optical noise. This type of noise may be greatly increased if some of the mirrors are not properly aligned, particularly those in the alternator section.

Figure 17 illustrates the different types of noise on the signal output when the instrument is adjusted to measure the formaldehyde concentration. The spectral bandpass has a halfwidth of  $15 \text{ cm}^{-1}$  and is centered at  $2803 \text{ cm}^{-1}$ . Three ballasts for the Nernst glower source were turned on to produce a source current of approximately 0.85 amp. The four upper strips were recorded with the multiple-pass sample cell adjusted to 40 passes and filled to 1 atm with nitrogen. The sample path-length and spectral bandpass are those recommended for maximum sensitivity and accuracy in measuring formaldehyde concentrations. The AGC was turned off, but the amplifier gain was manually adjusted to produce the same value of  $V_c$  that the AGC maintains. With the gain adjusted manually in this manner, it is possible to record the detector noise by blocking the chopped energy from the detector.

Each short strip in Figure 17 was cut from a longer strip recorded while monitoring the noise. The short strips, each corresponding to a 2-minute interval, were then pieced together. The output signal  $V'$  was adjusted to read zero before the recordings were traced. The plots were traced from right to left. As expected, the amplitude and the frequency of the noise decreased when the time constant was increased from 1 sec to 3 sec. The detector noise and optical noise combined are observed when the chopped signal is incident on the detector. With the sample cell adjusted to 40 passes, the noise obviously decreased when the radiant energy was blocked from the detector, indicating that the optical noise made a sizeable contribution to the combined noise.

The optical noise may increase to a level greater than that indicated in the upper right-hand panel if gas is flowing through the sample cell. This increase in noise is probably due to turbulence and is particularly noticeable if the incoming gas has a different composition, or is at a different temperature than the gas already in the cell.

The plots in the middle row were obtained in a similar manner but with the multiple-pass cell adjusted to 4 passes. More chopped energy was incident on the detector after the cell was set to 4 passes; therefore, the amplifier gain was reduced to maintain the same value of  $V_c$ . The detector noise observed with the detector blocked decreased in direct proportion to the decrease in amplifier gain. As with the cell adjusted to 40 passes, both the optical noise and detector noise contribute significantly to the combined noise when the time constant is 1 sec. Increasing the time constant reduces the detector noise to a

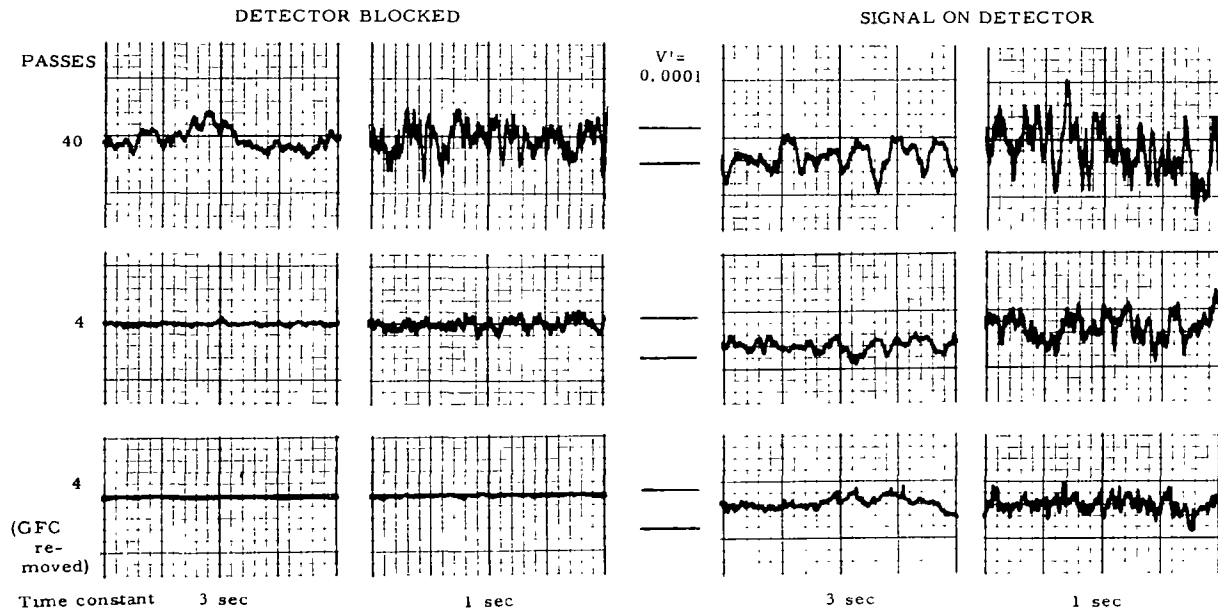


Figure 17. Recorder plots of the noise on the signal output for various operating conditions. Each short strip represents a 2 minute scan with the electronic time constant given below each section. The number of passes of the multiple-pass sample cell is indicated on the left-hand side of the figure. The recorder deflection corresponding to  $V' = 0.0001$  is the distance between the short parallel lines that have been drawn for reference in the middle of the figure.

very small value when the cell is at 4 passes. Much of the optical noise is apparently at a lower frequency and is not decreased as much by the increase in time constant.

The noise with the signal on the detector is seen to be approximately twice as much with the cell at 40 passes as at 4 passes. However, the sample path length is approximately 10 times greater at the higher number of passes. Therefore, the noise level is equivalent to a sample concentration 5 times as high at 4 passes as at 40 passes. It follows that the minimum detectable concentration is one-fifth as high at the longer path, provided that noise is the limiting factor. Of course, increasing the sample path-length will not improve the accuracy if it is limited by interference from other gases in the sample.

The four strips shown in the lower panel of Figure 17 were obtained with the GFC and the attenuators removed from the alternator section. When these components were removed, the amount of chopped energy incident on the detector increased by approximately a factor of 3. Thus the amplifier gains had to be reduced by this same factor in order to maintain  $V_c$  constant. The decrease in gain accounts for the decrease in noise observed with the detector blocked. With the GFC removed, the noise is much greater when the signal is on the detector than when the detector is blocked. Thus, the optical noise is much greater than the detector noise. Turbulence produced by the hot GFC when it is in place apparently does not contribute a major portion of the optical noise.

From the recorder plots shown in the upper right-hand corner of Figure 17, we conclude that noise limits the minimum detectable  $V'$  to approximately 0.0001 when the multiple-pass cell is adjusted to 40 passes (40 meters). From Equation (35) we see that this corresponds to a minimum detectable concentration of approximately 0.05 ppm of formaldehyde.

## SECTION XII

### MEASUREMENTS OF NH<sub>3</sub> AND VINYL CHLORIDE NEAR 1000 cm<sup>-1</sup>

#### EXPERIMENTAL ARRANGEMENT

Spectral curves of transmittance and data on the instrument sensitivity were obtained for NH<sub>3</sub> and vinyl chloride in order to determine the feasibility of a gas-filter correlation instrument to measure the two gases at low concentrations. Possible problems of interference were investigated, and data were obtained on sensitivity and noise levels. The work was limited to relatively small samples, and somewhat less care was exercised than would have been done if the data were intended for calibration of a finished instrument. The same experimental arrangement was employed for both of these two gases because they have strong infrared absorption features in the same spectral region. Figure 18 shows a spectral curve of transmittance for each of these gases along with a curve for ethylene, a gas that absorbs in the same spectral region and might interfere if it is present in the sample being studied. The two strong NH<sub>3</sub> absorption features near 931 cm<sup>-1</sup> and 966 cm<sup>-1</sup> were each investigated separately. The tests on vinyl chloride made use of the strong absorption near 942 cm<sup>-1</sup>. Previous tests in our laboratory had indicated that this absorption feature was stronger than the one near 897 cm<sup>-1</sup> and would result in better sensitivity if used in a vinyl chloride sensor.

Most of the measurements were made with the by-pass optics assembly in place so that the radiant energy beam did not go through the multiple-pass sample cell. A small, room-temperature cell, 0.43 cm long, was placed in the beam just ahead of the by-pass optics assembly. The GFC was 1 cm long and was located in the alternator section in the position indicated in Figure 1. Both the sample cell and the GFC contained NaCl windows. Lens L3 was not employed at the entrance slit of the grating section since no lens that was transparent in this spectral interval was available at the time. A 150 line/mm grating blazed at 1250 cm<sup>-1</sup> (8 μm) dispersed the energy so the desired spectral interval could be selected by the retroreflector-grid assembly. An interference filter that passes wavelengths greater than approximately 7.8 μm eliminated overlapping orders of energy of wavelengths shorter than those desired. The detector contained an HgCdTe element that was cooled to liquid-nitrogen temperature. Spectral curves of transmission and data on the instrument sensitivity and interference were obtained in the same manner as the formaldehyde data.

#### RESULTS FOR NH<sub>3</sub>

Two dilute mixtures of NH<sub>3</sub> + N<sub>2</sub> were used for the samples; one was 0.75% NH<sub>3</sub> and

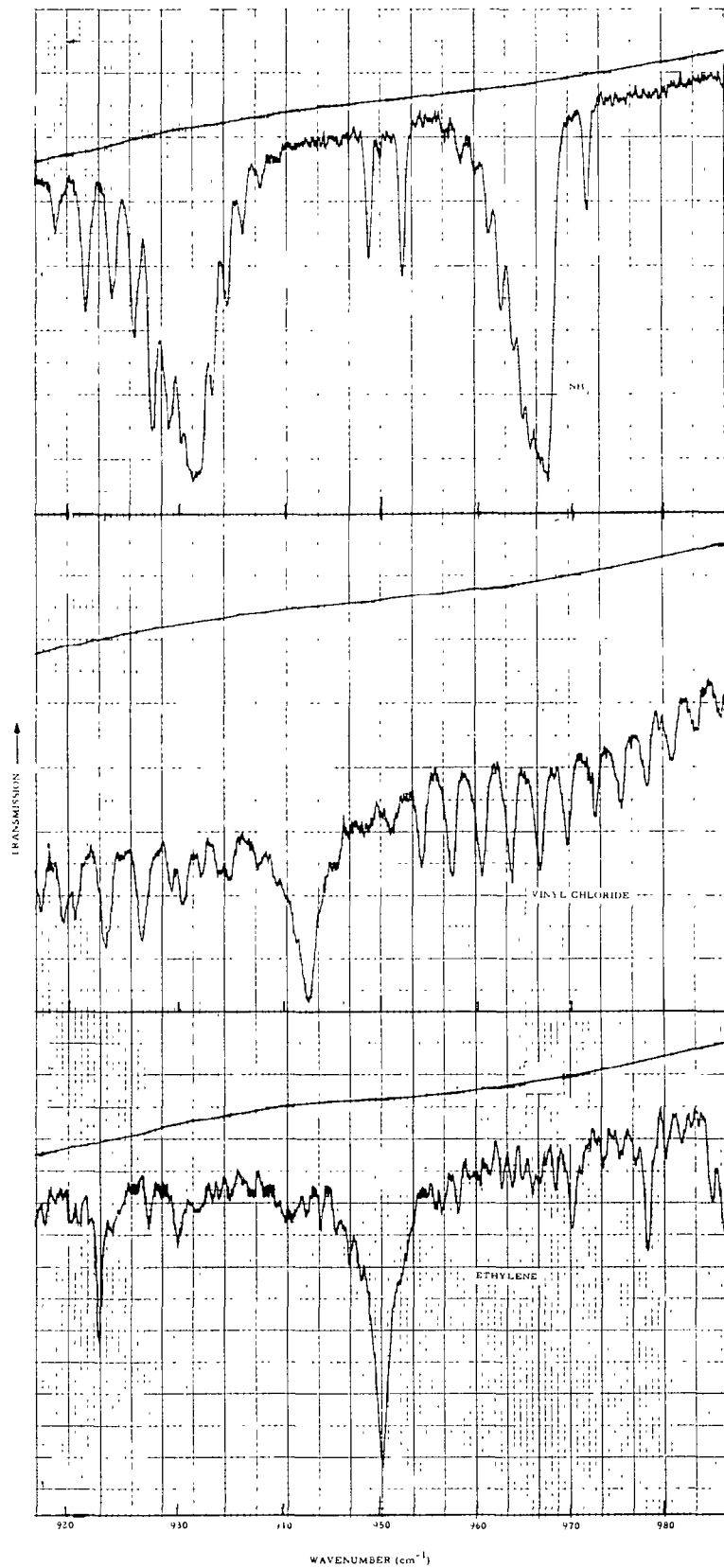


Figure 18. Spectral curves of transmittance of NH<sub>3</sub>, vinyl chloride, and ethylene between 920 and 985 cm<sup>-1</sup>. The curves were scanned with the versatile gas-filter spectrometer with no GFC in place.

the other was 3.3%  $\text{NH}_3$ . Each of these mixtures was studied at total pressures of approximately 0.2, 0.5, and 1 atm in the 0.43 cm sample cell. Samples were flushed slowly through the sample cell for several seconds before the valves were closed and the measurement was made. This allowed adsorption of  $\text{NH}_3$  on the walls to take place and approach equilibrium so that the concentration of the mixture in the sample would be close to that in the container from which the mixture was drawn. Longer periods would be required for adsorption to come to equilibrium if high accuracy were required. The estimated combined uncertainty in the absorber thickness of the samples due to adsorption and errors in pressure measurement is less than  $\pm 10\%$ , which was adequate for the preliminary tests being performed.

The majority of the data were obtained with the grating assembly adjusted to pass a narrow spectral band that included the strong Q-branch near  $966\text{ cm}^{-1}$ . Two different grids were employed in the retroreflector-grid assembly. The wider one (10 mm) passed a spectral interval approximately  $7.2\text{ cm}^{-1}$  wide at  $966\text{ cm}^{-1}$  and  $6.2\text{ cm}^{-1}$  wide at  $931\text{ cm}^{-1}$ . The corresponding bandpasses are  $2.9$  and  $2.5\text{ cm}^{-1}$  for the other grid, which had a narrower, 4 mm opening. The entrance slit was 1.6 mm wide for all of the gas-filter correlation data. A few data obtained for the other Q-branch near  $931\text{ cm}^{-1}$  indicated that this region did not produce sensitivity quite as high as the other wavenumber region. The dependence of the correlation efficiency  $C_e$  (see Equation (13)) and the Pembroke factor,  $F$ , on the parameters of the gas-filter cell (GFC) was also investigated.

Table 2 summarizes the data obtained for  $\text{NH}_3$ . Each group corresponds to a given spectral bandpass and a fixed set of GFC parameters with different sample total pressures. The GFC was filled with  $\text{NH}_3 + \text{N}_2$  mixtures at different concentrations to provide the total pressures and values of  $\bar{T}_g$  shown in Table 2. Nearly all of the samples studied produced values of  $\bar{A}_{at,s}$  less than 0.25 and  $V'$  less than 0.03. For samples absorbing this little,  $C_e$  and  $F$  are essentially independent of the absorber thickness as long as the total pressure is constant. Each set of conditions shown in Table 2 represents data for from one to five samples. Values of  $C_e$  have been rounded off to the nearest 0.05 or 0.10 except for values less than 0.20, for which the rounding was to the nearest 0.00, 0.02, 0.05, or 0.07. Values of  $F$  have been rounded off accordingly and are believed to be accurate to between  $\pm 10\%$  and  $\pm 20\%$ .

If the GFC is at 1 atm, the results of group A indicate that  $C_e$  is independent, within the accuracy of the present experiment, of sample pressure if it is less than 1 atm. However, if the GFC is at 0.2 atm,  $C_e$  is higher for low-pressure samples than for samples near 1 atm. Correlation efficiencies as high as 0.6 are observed when both the GFC and the sample cell are at 0.2 atm. This result can be explained on the basis of pressure broadening of the many individual lines that appear in the spectral bandpass. At the higher pressures, the lines overlap each other, smoothing out much of the spectral structure on which the GFC method depends for its sensitivity. When  $\bar{T}_g$ , the average transmittance of the GFC, is approximately 0.7,  $C_e$  is not as high as when  $\bar{T}_g$  is lower. The higher value of  $C_e$  results because the GFC corresponding to the lower  $\bar{T}_g$  is more nearly opaque at the wavenumbers where the sample absorbs. In accordance with the discussion of Section V, this increases the correlation efficiency.

Larger values of  $C_e$  are observed with the  $7.2\text{ cm}^{-1}$  spectral bandpass than with the narrow  $2.9\text{ cm}^{-1}$  bandpass. The narrower interval contains strong lines

TABLE 2

SUMMARY OF DATA ON NH<sub>3</sub> SENSITIVITY

Group	Spectral Bandpass		GFC		Sample	C <sub>e</sub>	F <sup>(a)</sup> (atm cm) <sup>-1</sup>
	$\nu$ (cm <sup>-1</sup> )	$\Delta\nu$ (cm <sup>-1</sup> )	P (atm)	$\bar{T}_g$	P (atm)		
A	966	7.2	1.0	0.5	1.0	0.40	2.2
A	966	7.2	1.0	0.5	0.5	0.40	2.2
A	966	7.2	1.0	0.5	0.2	0.40	2.2
B	966	7.2	0.2	0.5	1.0	0.40	2.2
B	966	7.2	0.2	0.5	0.5	0.50	2.7
B	966	7.2	0.2	0.5	0.2	0.60	3.3
C	966	7.2	1.0	0.7	1.0	0.20	1.1
C	966	7.2	1.0	0.7	0.5	0.20	1.1
C	966	7.2	1.0	0.7	0.2	0.20	1.1
D	966	7.2	0.2	0.7	1.0	0.25	1.3
D	966	7.2	0.2	0.7	0.5	0.35	2.0
D	966	7.2	0.2	0.7	0.2	0.60	3.3
E	966	2.9	1.0	0.6	1.0	0.10	1.0
E	966	2.9	1.0	0.6	0.5	0.13	1.3
E	966	2.9	1.0	0.6	0.2	0.17	1.7
F	966	2.9	0.2	0.7	1.0	0.10	1.0
F	966	2.9	0.2	0.7	0.5	0.15	1.5
F	966	2.9	0.2	0.7	0.2	0.30	3.0
G	966	2.9	0.2	0.5	1.0	0.15	1.5
G	966	2.9	0.2	0.5	0.5	0.30	3.0
G	966	2.9	0.2	0.5	0.2	0.60	6.0
H	931	6.2	0.2	0.7	1.0	0.15	0.8
H	931	6.2	0.2	0.7	0.5	0.25	1.4
H	931	6.2	0.2	0.7	0.2	0.45	2.5
I	931	6.2	0.2	0.5	1.0	0.30	1.6
I	931	6.2	0.2	0.5	0.5	0.40	2.2
I	931	6.2	0.2	0.5	0.2	0.50	2.7

(a)  $F = C_e \bar{k}_s / 2 = V/u$  for small absorptance.

$\bar{k}_s = 11$  (atm cm)<sup>-1</sup> for 7.2 cm<sup>-1</sup> interval at 966 cm<sup>-1</sup> and 6.2 cm<sup>-1</sup> interval at 931 cm<sup>-1</sup>, and 20 (atm cm)<sup>-1</sup> for the 2.9 cm<sup>-1</sup> interval at 966 cm<sup>-1</sup>.

throughout most of its width and therefore must depend on the structure between the closely spaced lines. Thus,  $C_e$  is very low when either the sample or the GFC is at 1 atm or higher. On the other hand, the  $7.2 \text{ cm}^{-1}$  interval is wide enough to include some of the region of weak absorption next to the strong lines in the Q-branch. Thus, some spectral structure remains within the spectral interval, even when much of the structure between the lines is filled in. Use of spectral intervals 15 or  $20 \text{ cm}^{-1}$  wide that include one of the Q-branches would probably produce slightly larger values of  $C_e$  than those obtained with the  $7.2 \text{ cm}^{-1}$  interval. However, the average absorption coefficient,  $\bar{k}_s$  (Equation (20)), is correspondingly less for the wider interval. As a result, the important Pembroke factor,  $F$ , is not expected to increase significantly as the bandpass increases beyond  $7.2 \text{ cm}^{-1}$ . As the interval becomes more than 2 or 3 times the width of the Q-branch, the value of  $F$  will decrease because of the corresponding decrease in  $\bar{k}_s$ . In summary, the  $7.2 \text{ cm}^{-1}$  interval is probably near the optimum for maximum  $F$ .

After the grid was placed in the retroreflector-grid assembly to fix the width of the spectral bandpass, the grating screw was adjusted to make a slight change in  $\nu_c$ , the center of the interval, to minimize the transmittance of the GFC. Adjusting the location of the bandpass in this manner makes the instrument stability less susceptible to small changes in the spectral bandpass due to temperature changes or to stresses on the instrument. At the possible expense of some stability, some increase in  $C_e$  and  $F$  might be gained by shifting  $\nu_c$  a small fraction of the bandwidth toward higher wavenumbers than those used in the experiment.

As one might expect from the spectral curves in Figure 18, ethylene interferes with the measurement of ammonia. The discrimination ratio for ethylene varied from approximately -10 to -30, depending on the pressures of the sample and the GFC. The greatest interference, corresponding to the lowest discrimination ratio, was observed when both the GFC and sample were at 1 atm. Better discrimination was observed when both cells were at 0.2 atm. The interference was approximately the same at  $931 \text{ cm}^{-1}$  as at  $966 \text{ cm}^{-1}$ . Only the narrow spectral bandpass, approximately  $2.9 \text{ cm}^{-1}$ , was employed in the ethylene interference measurements.

Interference by  $\text{H}_2\text{O}$  is certain to be slight, and possibly insignificant, because absorption by this gas in this spectral region is known to be very weak. Furthermore, most of the  $\text{H}_2\text{O}$  absorption that does occur is due to continuum absorption against which a GFC instrument has good discrimination. Any possible  $\text{H}_2\text{O}$  interference that might occur can easily be accounted for electronically by the  $\text{H}_2\text{O}$  monitor.

A one-atmosphere sample of 14.5%  $\text{CO}_2$  in  $\text{N}_2$  was introduced into the multiple-pass sample cell when it was adjusted to 40 meters. The spectral bandpass and GFC corresponded to data Group B in Table 2. The slight response of the instrument to this large  $\text{CO}_2$  sample indicated a discrimination ratio against  $\text{CO}_2$  of about 800,000:1. A 16% mixture of  $\text{CO}_2$ , which is about as rich as ever occurs in auto exhaust, would produce an error equivalent to 0.2 ppm of  $\text{NH}_3$ . By adjusting some of the instrument parameters, the small amount of interference could likely be reduced even further if it produced serious error. The  $\text{CO}_2$  concentration is frequently known with fair accuracy so that the residual  $\text{CO}_2$  interference could be calculated and accounted for.

We now consider the performance that we might expect from a GFC analyzer built

specifically for  $\text{NH}_3$ . Assume that the samples are kept at 1 atm in a multiple-pass sample cell similar to the one in the present instrument with a one-meter baselength and a total path length of 40 meters. The results obtained with formaldehyde indicated that a practical minimum lower limit of  $V' = 10^{-4}$  is imposed by optical instabilities and turbulence in the multiple-pass sample cell. From the results summarized in Table 2, we see that we can expect a Pembroke factor  $F = 2$ . Thus the minimum detectable absorber thickness that is imposed by a minimum  $V'$  of  $10^{-4}$  is  $10^{-4}/2 = 0.5 \times 10^{-4}$  atm cm. In a 4000 cm cell, this corresponds to a minimum detectable concentration of  $(0.5 \times 10^{-4})/4000 = 1.25 \times 10^{-8}$  atm cm = 0.0125 ppm.

This very good sensitivity is, of course, dependent on having an optical system with high energy throughput, a good source and a detector with high detectivity so that the instrument sensitivity is not limited by detector noise or amplifier noise. The present instrument is limited by the noise from the HgCdTe detector. With the bandpass adjusted as it was when obtaining the data for Group B in Table 2, a time-constant of 3 seconds, and the multiple-pass cell adjusted to 40 meters, the noise-level corresponded to  $V' = 0.003$ . By comparing this with the results from the previous paragraph, we see that this corresponds to a minimum detectable concentration of approximately 0.4 ppm.

Better detectivity than this could be obtained with the same type of instrument by making a few changes. For example, it is probably possible to gain a factor of approximately 4 or 5 by decreasing the size of the detector element and paying a premium price for a detector with higher detectivity. Installing a cold-filter in the detector dewar just ahead of the sensitive element could further improve the detectivity by decreasing the amount of background energy incident on the detector. Gains of 2 to 4 could also be obtained by different methods of increasing the energy throughput. In summary, it appears that a minimum detectable  $\text{NH}_3$  concentration as low as 0.02 to 0.04 ppm could be obtained with a GFC instrument employing the  $966 \text{ cm}^{-1}$  absorption feature and a multiple-pass absorption cell. The instrument could easily fit on a table-top and be easy to use and make nearly real-time measurements with a response time of a few seconds. Even further reductions in the minimum detectable concentration to less than 0.01 ppm with such an instrument does not appear to be unrealistic.

## RESULTS FOR VINYL CHLORIDE

The data obtained on vinyl chloride are summarized in Table 3 in the same way that the  $\text{NH}_3$  data are summarized above. Two different spectral intervals were employed; both were centered near the strong absorption at approximately  $942 \text{ cm}^{-1}$ . The dependence of  $C_e$  and of  $F$  on spectral slitwidth, average transmittance  $\bar{T}_g$  of the GFC, and sample pressure are similar to those observed with  $\text{NH}_3$ . The highest values of  $C_e$  and  $F$  are obtained with low values of  $\bar{T}_g$ . The optimum value of  $\bar{T}_g$  for a particular instrument depends on other factors, including detector noise. Further decreasing of  $\bar{T}_g$  below values represented in the table would probably result in additional increases in  $C_e$  and  $F$ . However, the decrease in  $\bar{T}_g$  reduces the amount of energy reaching the detector; thus, the detector noise becomes a bigger factor.

Comparison of data Groups E and G in the table shows that  $C_e$  has little, if any, dependence on the pressure of the gas in the GFC when the spectral interval is wide enough to include the strong absorption and some weaker absorption on

TABLE 3

## SUMMARY OF DATA ON VINYL CHLORIDE SENSITIVITY

Group	Spectral Bandpass		GFC		Sample	$c_e$	$F^{(b)}$ (atm cm) <sup>-1</sup>
	$\nu_c$ (cm <sup>-1</sup> )	$\Delta\nu$ (cm <sup>-1</sup> )	$P^{(a)}$ (atm)	$\bar{T}_g$	P (atm)		
A	942	2.6	.06	.75	1.0	0.07	.20
A	942	2.6	.06	.75	0.5	0.10	.28
A	942	2.6	.06	.75	0.2	0.15	.40
B	942	2.6	.15	.47	1.0	0.17	.50
B	942	2.6	.15	.47	0.5	0.25	.70
B	942	2.6	.15	.47	0.2	0.30	.85
C	942	2.6	.26	.31	1.0	.30	.85
C	942	2.6	.26	.31	0.5	.30	.85
D	942	6.5	.10	.73	1.0	.15	.28
D	942	6.5	.10	.73	0.5	.17	.32
D	942	6.5	.10	.73	0.2	.20	.37
E	942	6.5	.20	.55	1.0	.25	.46
E	942	6.5	.20	.55	0.5	.25	.46
E	942	6.5	.20	.55	0.2	.25	.46
F	942	6.5	.36	.35	1.0	.30	.56
F	942	6.5	.36	.35	0.5	.30	.56
G	942	6.5	1.0	.55	1.0	.25	.46

(a) Pure vinyl chloride was used in the GFC for groups A through F; a mixture of vinyl chloride plus nitrogen was used for G.

(b)  $F = C_e \bar{k}_s / 2 = V/u$  for small absorbance.

$\bar{k}_s = 5.6 \text{ (atm cm)}^{-1}$  for the  $2.6 \text{ cm}^{-1}$  interval and  $3.7 \text{ (atm cm)}^{-1}$  for the  $6.5 \text{ cm}^{-1}$  interval.

either side. Group A includes data obtained with a narrow,  $2.6 \text{ cm}^{-1}$ , spectral interval and a relatively small amount of vinyl chloride in the GFC to produce  $\bar{T}_g = 0.75$ . In this case the transmittance is low only very near the centers of the strongest lines, and the instrument sensitivity is dependent on the structure between the closely-spaced lines. At low pressures, the lines are narrow and there is more structure than occurs at higher gas pressures. For  $\bar{T}_g$  as high as 0.75,  $C_e$  is very low except when the pressures in both the GFC and the sample are low.

A few data were obtained on the interference by ethylene, ammonia,  $\text{CO}_2$  and  $\text{H}_2\text{O}$  with the spectral bandpass and the GFC parameters similar to those in data Group E in Table 3. The discrimination ratios were observed to be greater than 50,000:1 for both  $\text{CO}_2$  and  $\text{H}_2\text{O}$ . The  $\text{H}_2\text{O}$  interference was not determined reliably; the discrimination ratio may be much greater than 50,000:1. Any interference by this gas that might occur could easily be accounted for by an  $\text{H}_2\text{O}$  monitor with automatic correction circuitry similar to that in the instrument being reported here. The largest sample of  $\text{NH}_3$  investigated for interference consisted of 1 atm of pure ammonia in a 0.43 cm cell. The absorptance,  $\bar{A}_{at,s}$ , of this sample was approximately 0.20. However, the correlation of the spectral structure of the  $\text{NH}_3$  and vinyl chloride is apparently low because this produced a  $V'$  of 0.003 and a corresponding discrimination ratio of approximately -100:1. Absorption by ethylene is also strong in this spectral region, and its discrimination ratio is approximately 70:1. Although the discrimination ratios for ethylene and ammonia are relatively low, their concentrations are expected to be low in most places where vinyl chloride is being monitored; therefore, the interference would probably not be serious.

In order to estimate the performance of a GFC instrument designed specifically for vinyl chloride, we can compare the results with those for ammonia. For vinyl chloride, we can expect  $F$  to be approximately 0.7 for 1 atm samples and a  $6.5 \text{ cm}^{-1}$  spectral interval. This is 0.35 as high as the values assumed above for  $\text{NH}_3$ ; thus the estimated minimum detectable concentration of vinyl chloride is approximately 3 times as high as for  $\text{NH}_3$ . With the present instrument adjusted for a 40 meter path-length, the minimum detectable concentration is approximately 1 ppm. However, by making some of the changes discussed above with regard to  $\text{NH}_3$ , this quantity can probably be reduced to less than 0.1 ppm.

## SECTION XIII

### REFERENCES

1. Burch, D. E., and J. D. Pembroke. "Instrument to Monitor CH<sub>4</sub>, CO, and CO<sub>2</sub> in Auto Exhaust." Prepared by Philco-Ford Corporation for EPA under Contract No. 68-02-0587. EPA Report No. 650/2-73-030, October 1973.
2. Burch, D. E., and D. A. Gryvnak. "Infrared Gas Filter Correlation Instrument for In-Situ Measurement of Gaseous Pollutants." Prepared by Philco-Ford Corporation for EPA under Contract No. 68-02-0575. EPA Report No. EPA-650/2-74-094. Also, Burch, D. E., and D. A. Gryvnak. "Cross-Stack Measurement of Pollutant Concentrations Using Gas-Cell Correlation Spectroscopy." Chapter 10 of Analytical Methods Applied to Air Pollution Measurements, Stevens, R. K. and W. F. Herget, (eds.). Ann Arbor, Ann Arbor Science Publishers Inc., 1974.
3. Burch, D. E. "Adjustable Bandpass Filter Employing a Prism." Appl. Optics 8, 649 (1969).
4. White, John U. "Long Optical Paths of Large Aperture." Journ. of the Optical Society of America 32:285-288, May 1942.
5. Decker, J. A. Jr. "Experimental Realization of the Multiplex Advantage with a Hadamard-Transform Spectrometer." Appl. Opt. 10, No. 3, 510-514, 1971.

**TECHNICAL REPORT DATA**  
(Please read Instructions on the reverse before completing)

1. REPORT NO EPA-600/2-75-024		2.	3. RECIPIENT'S ACCESSION NO	
4. TITLE AND SUBTITLE  VERSATILE GAS FILTER CORRELATION SPECTROMETER			5. REPORT DATE	
			6. PERFORMING ORGANIZATION CODE	
7. AUTHOR(S) D. E. Burch, F. J. Gates, D. A. Gryvnak, J. D. Pembroke			8. PERFORMING ORGANIZATION REPORT NO  U-6201	
9. PERFORMING ORGANIZATION NAME AND ADDRESS Aeronutronic Ford Corporation Aeronutronic Division Ford Road Newport Beach, Calif. 92663			10. PROGRAM ELEMENT NO. P.E. 1A1010 (ROAP 26 ACV)	
			11. CONTRACT/GRANT NO.  68-02-1227	
12. SPONSORING AGENCY NAME AND ADDRESS Environmental Sciences Research Laboratory Office of Research and Development U.S. Environmental Protection Agency Research Triangle Park, North Carolina 27711			13. TYPE OF REPORT AND PERIOD COVERED Final: June '73 - June '75	
			14. SPONSORING AGENCY CODE  EPA - ORD	
15. SUPPLEMENTARY NOTES				
16. ABSTRACT  A versatile infrared analyzer employing gas-filter correlation techniques has been designed and constructed to measure concentrations of pollutant gases from a variety of sources. The spectral bandpass is determined by an adjustable grating assembly. By interchanging cell windows, radiant energy sources, gratings, interference filters, and detectors, nearly any desired spectral bandpass between 0.3 μm and 11 μm can be obtained. Spectral curves of transmittance can also be scanned. A multiple-pass sample cell provides sample paths between approximately 4 m and 40 m. Shorter sample cells can also be employed. An H <sub>2</sub> O monitor measures the concentration of H <sub>2</sub> O in the multiple-pass sample cell and automatically accounts for interference by H <sub>2</sub> O in the measurement of other gas concentrations. Tests have been performed on the measurement of formaldehyde, vinyl chloride and ammonia. The minimum detectable concentration of formaldehyde in automotive exhaust is approximately 0.05 ppm.				
17. KEY WORDS AND DOCUMENT ANALYSIS				
a. DESCRIPTORS		b. IDENTIFIERS/OPEN ENDED TERMS		c. COSATI Field/Group
* Spectrometer * Exhaust gases Air pollution Formaldehyde Vinyl chloride		Ammonia  Gas-filter correlation		14B 13B 21B 07C 07B
18. DISTRIBUTION STATEMENT  Release to public		19. SECURITY CLASS (This Report)  Unclassified		21. NO. OF PAGES  76
		20. SECURITY CLASS (This page)  Unclassified		22. PRICE

ENVIRONMENTAL PROTECTION AGENCY  
Technical Publications Branch  
Office of Administration  
Research Triangle Park, North Carolina 27711

OFFICIAL BUSINESS

AN EQUAL OPPORTUNITY EMPLOYER

POSTAGE AND FEES PAID .  
ENVIRONMENTAL PROTECTION AGENCY  
EPA - 335

EPA 600/2-75-024

Return this sheet if you do NOT wish to receive this material .  
or if change of address is needed . (Indicate change, including  
ZIP code.)

PUBLICATION NO. EPA-600/2-75-024